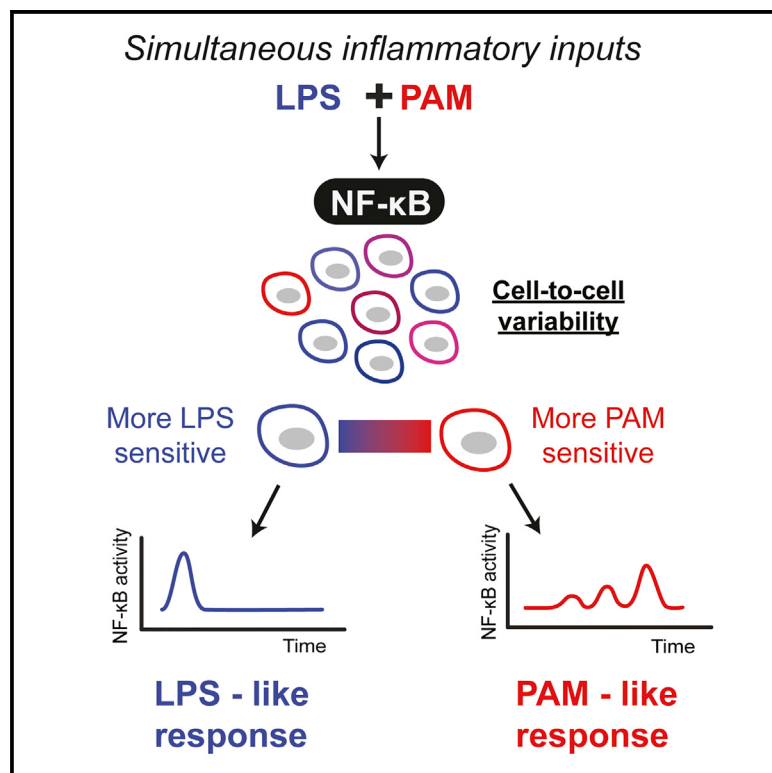


Cellular Decision Making by Non-Integrative Processing of TLR Inputs

Graphical Abstract



Authors

Ryan A. Kellogg, Chengzhe Tian,
Martin Etzrodt, Savaş Tay

Correspondence

tays@uchicago.edu

In Brief

Kellogg et al. study NF-κB responses under TLR co-stimulation and observe that single cells respond with a dynamic NF-κB profile characteristic of either TLR2 or TLR4 activation, rather than a mixed response. Modeling and microfluidic experiments revealed that switch-like NF-κB activation and TLR cross-tolerance mediate this phenomenon, termed non-integrative processing.

Highlights

- Bacterial infection involves co-stimulation of TLR4 and TLR2 receptors
- TLR4 and TLR2 induced distinct dynamic NF-κB profiles when stimulated separately
- Under co-stimulation, single cells responded to either one ligand or the other
- Switch-like NF-κB response and TLR cross-tolerance mediate non-integrative processing



Cellular Decision Making by Non-Integrative Processing of TLR Inputs

Ryan A. Kellogg,^{1,5,6} Chengzhe Tian,^{2,6} Martin Etzrodt,¹ and Savaş Tay^{1,3,4,7,*}

¹Department of Biosystems Science and Engineering, ETH Zürich 4058, Switzerland

²Niels Bohr Institute, University of Copenhagen, 2100 Copenhagen, Denmark

³Institute for Molecular Engineering, University of Chicago, Chicago, IL 60637, USA

⁴Institute for Genomics and Systems Biology, University of Chicago, Chicago, IL 60637, USA

⁵Department of Genetics, Stanford University School of Medicine, Stanford, CA 94305, USA

⁶Co-first author

⁷Lead Contact

*Correspondence: tays@uchicago.edu

<http://dx.doi.org/10.1016/j.celrep.2017.03.027>

SUMMARY

Cells receive a multitude of signals from the environment, but how they process simultaneous signaling inputs is not well understood. Response to infection, for example, involves parallel activation of multiple Toll-like receptors (TLRs) that converge on the nuclear factor κ B (NF- κ B) pathway. Although we increasingly understand inflammatory responses for isolated signals, it is not clear how cells process multiple signals that co-occur in physiological settings. We therefore examined a bacterial infection scenario involving co-stimulation of TLR4 and TLR2. Independent stimulation of these receptors induced distinct NF- κ B dynamic profiles, although surprisingly, under co-stimulation, single cells continued to show ligand-specific dynamic responses characteristic of TLR2 or TLR4 signaling rather than a mixed response, comprising a cellular decision that we term “non-integrative” processing. Iterating modeling and microfluidic experiments revealed that non-integrative processing occurred through interaction of switch-like NF- κ B activation, receptor-specific processing timescales, cell-to-cell variability, and TLR cross-tolerance mediated by multilayer negative feedback.

INTRODUCTION

Cells process signals through shared signaling networks that relay information from outside the cell to make decisions. Although cells can handle a remarkable number of parallel signals, it is not well understood how cells process distinct simultaneous inputs through the same pathway. Signaling pathways mediate gene regulation through dynamic activation of transcription factors, and transcription factor dynamics transmit stimulus information through specific gene expression responses to

distinct pathway inputs (Behar et al., 2013; Cheong et al., 2011; Selimhanov et al., 2014). For example, in the nuclear factor κ B (NF- κ B) system, distinct responses to lipopolysaccharide (LPS) and tumor necrosis factor (TNF) occur due to altered dynamic profiles of I κ B kinase (IKK) and NF- κ B activation (Werner et al., 2005). Therefore, signaling dynamics mediate ligand-specific responses through the NF- κ B pathway.

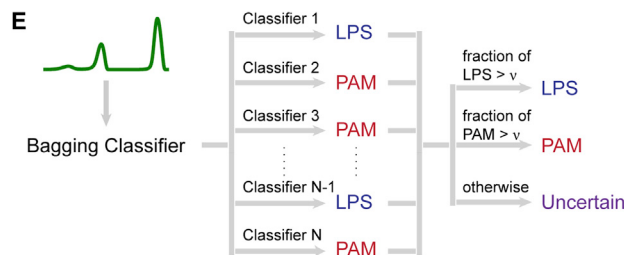
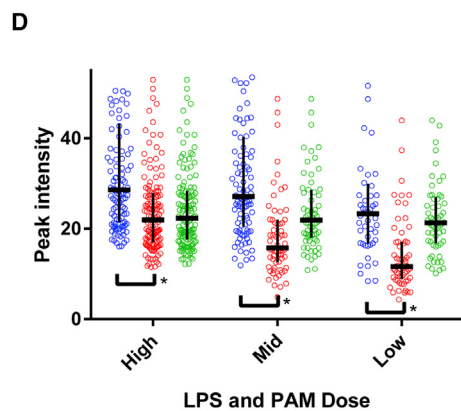
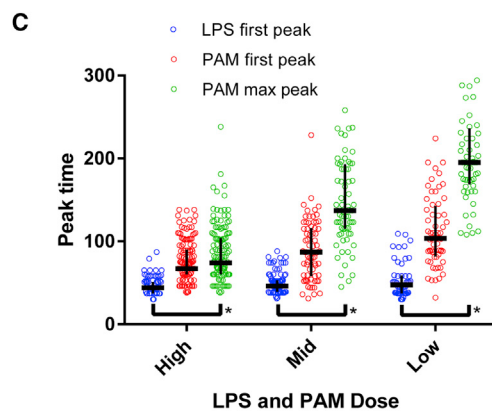
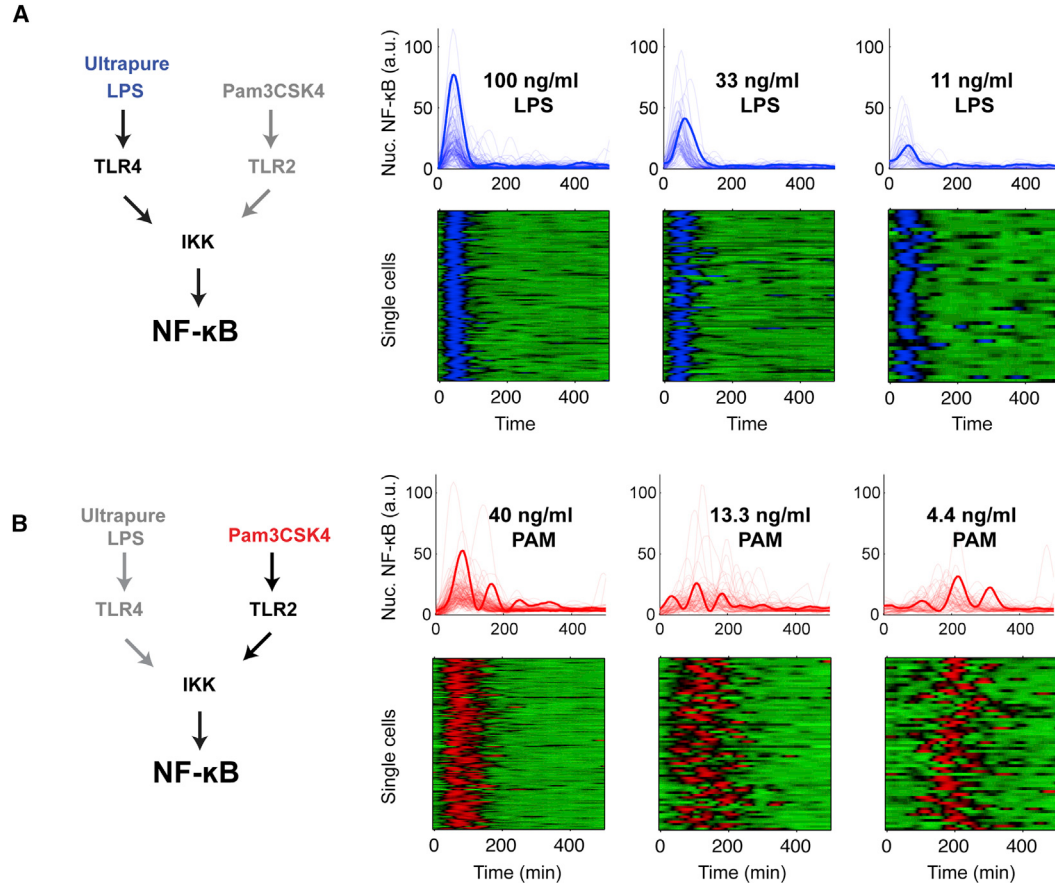
Cells increase decision robustness in the presence of noise through switch-like responses (Ferrell and Machleder, 1998; Liu et al., 2014; Malleshaiah et al., 2010; Shah and Sarkar, 2011). The NF- κ B system exhibits switch-like activation at the single cell level in B and T cells in addition to non-immune cells (Kingeter et al., 2010; Shinohara et al., 2014; Tay et al., 2010). We recently showed that integration of signal intensity and duration determines the probability of NF- κ B switch activation (Kellogg et al., 2015). During infection, multiple pathogen-associated molecules activate NF- κ B through Toll-like receptor signaling (Akira and Takeda, 2004; Takeda and Akira, 2005). For example, Toll-like receptor (TLR)4 and TLR2 recognize different cell wall components during bacterial infection and may be activated simultaneously, sharing the same downstream NF- κ B signal processing apparatus (Kopp and Medzhitov, 2003; Takeuchi et al., 1999). While NF- κ B exhibits switch-like response to single ligands in isolation, it is not clear how switch-like activation occurs in the physiological situation of multiple simultaneous pathogen-associated input signals to the NF- κ B pathway.

To study information processing through the NF- κ B pathway under multiple concurrent input signals, we used an automated microfluidic cell culture platform to generate combinatorial TLR2 and TLR4 pathway stimulation and monitored NF- κ B dynamics by live imaging (Kellogg et al., 2014). Lipoglycans and bacterial lipoproteins make up the cell wall of bacteria and simultaneous delivery of these two inputs to mammalian cells simulates an infection scenario (Philpott and Girardin, 2004). We found that when TLR4 and TLR2 were stimulated independently by specific agonists ultrapure-LPS for TLR4 and Pam3CSK4 (PAM) a synthetic triacylated lipopeptide for TLR2 activation, distinct (“LPS-like” or “PAM-like”) dynamic NF- κ B profiles appeared in single cells. Surprisingly, under TLR2-TLR4 co-stimulation, we discovered that most single cells exhibited an NF- κ B



CrossMark

Cell Reports 19, 125–135, April 4, 2017 © 2017 The Author(s). 125
This is an open access article under the CC BY-NC-ND license (<http://creativecommons.org/licenses/by-nc-nd/4.0/>).



F

	LPS 100 PAM 40	LPS 33 PAM 13.3	LPS 11 PAM 4.4
Correct	85.6%	87.3%	86%
Incorrect	6.5%	6.2%	5.9%
Uncertain	7.9%	6.5%	7.8%

(legend on next page)

response characteristic of either TLR4 activation or TLR2 activation, rather than a response combining dynamic features of both pathways. These results suggest that switch-like activation enables cells to respond with a dynamic signature corresponding to a specific ligand although multiple are present.

RESULTS

Independent TLR Stimulation Induces Distinct NF- κ B Dynamic Signatures in Single Cells

We first asked whether different bacteria-associated molecules induce distinct NF- κ B dynamics (Ozinsky et al., 2000; Takeda and Akira, 2005). Both TLR2 and TLR4 activate the NF- κ B pathway via adaptor proteins including TRAF6 to induce IKK activation, which causes degradation of inhibitor of κ B (IkB) and NF- κ B translocation from the cytoplasm to the nucleus. NF- κ B induces expression of hundreds of genes including its inhibitor IkB, creating negative feedback and oscillations in cytoplasm-nucleus NF- κ B translocation (Hoffmann et al., 2002). Because dynamics of transcription factor activation were previously shown to encode stimulus-specific information (Behar et al., 2013; Caldwell et al., 2014; Selimkhanov et al., 2014; Werner et al., 2005), we hypothesized that different TLR ligands would induce distinct NF- κ B dynamic profiles.

We independently activated TLR4 or TLR2 using ultrapure LPS (LPS) or PAM, respectively, at three dose levels for each ligand (Figures 1A and 1B) spanning the physiological response range (Simmons et al., 2010; Tay et al., 2010). We applied these six conditions using microfluidic cell culture (Gómez-Sjöberg et al., 2007; Kellogg et al., 2014; Kellogg and Tay, 2015) and observed NF- κ B cytoplasm-nucleus translocation dynamics by live imaging in single mouse fibroblast cells expressing NF κ B(p65)-DsRed fusion protein at near-endogenous levels (Tay et al., 2010). LPS stimulation activating only TLR4 led to a single-peak response with decreasing amplitude and cell-to-cell timing variability with lower dose (Figures 1A, 1C, and 1D). In contrast, PAM stimulation causing TLR2 activation led to markedly variable dynamics between cells, with a pronounced delay with decreased dose. While PAM activated all cells, LPS

activated a fraction of the population in the concentrations tested (Table S6). Moreover, the low-dose PAM response exhibited oscillations with increasing amplitude over time, followed by a rapid shut-off in the NF- κ B response 300–400 min post-stimulus (Figures 1B–1D).

We sought to test whether LPS- and PAM-specific responses are distinguishable based on single-cell NF- κ B dynamics. We trained a classifier using the experimental trajectories for LPS and PAM responses at each dose level and asked whether test trajectories could be correctly separated into “LPS-like” or “PAM-like” classes (Dietterich, 2000) (Figure 1E; Supplemental Experimental Procedures). In the classification approach (called a bagging classifier), an ensemble of decision trees determines whether a test trajectory is more similar to LPS-like, PAM-like, or uncertain (interpreted as mixed response) (Figure S1). We used artificial “mixed” trajectories to check for classifier bias (Figures S1D and S1E). This analysis found that NF- κ B trajectories could be reliably separated into LPS-like or PAM-like classes, with ~85% of the single-cell traces correctly discriminated and less than 10% having uncertain or mixed classification (Figure 1F). These results indicate that distinct NF- κ B dynamics encode TLR2 (PAM) and TLR4 (LPS) pathway stimulation.

Distinct TLR-NF- κ B Profiles Arise through Receptor-Specific Processing and Feedback Dynamics

To understand how TLR-specific NF- κ B dynamics arise, we expanded our previous model of LPS/TLR4-mediated NF- κ B signaling to additionally incorporate the PAM/TLR2 pathway branch (Kellogg et al., 2015). At the receptor level, TLR4 and TLR2 have similar structure: both receptor groups signal through MyD88 and TRAF6 to cause IKK and NF- κ B activation (Figure 2E). While LPS initiates MyD88 signaling from the cell membrane, PAM signaling initiates MyD88 signaling from endosomes following receptor-ligand internalization (Brandt et al., 2013; Dietrich et al., 2010; Stack et al., 2014). Model with slowed accumulation of TRAF6 in TLR2 signaling due to endosomal processing reproduced the increasing-amplitude NF- κ B oscillations observed experimentally (Figure 2A).

Figure 1. Distinct NF- κ B Pathway Dynamics Induced by TLR4 and TLR2 Engagement

Ultrapure LPS (LPS) and PAM that activate TLR4 and TLR2, respectively, were applied in three concentrations to fibroblasts using automated microfluidic cell culture, and NF- κ B dynamic activation was measured in single cells by live-cell microscopy.

(A) Single-cell NF- κ B dynamic profiles of cells stimulated with LPS in microfluidic chambers, shown in line plots (upper row) and heatplots (lower row). Each row of the heatplot corresponds to one cell, with color indicating nuclear NF- κ B (green, low; blue, high). As ultrapure dose decreases, there is a corresponding decrease in response amplitude (bolded line, example cell in each dose condition). Only nuclear NF- κ B time courses of active cells are plotted in the heatplot.

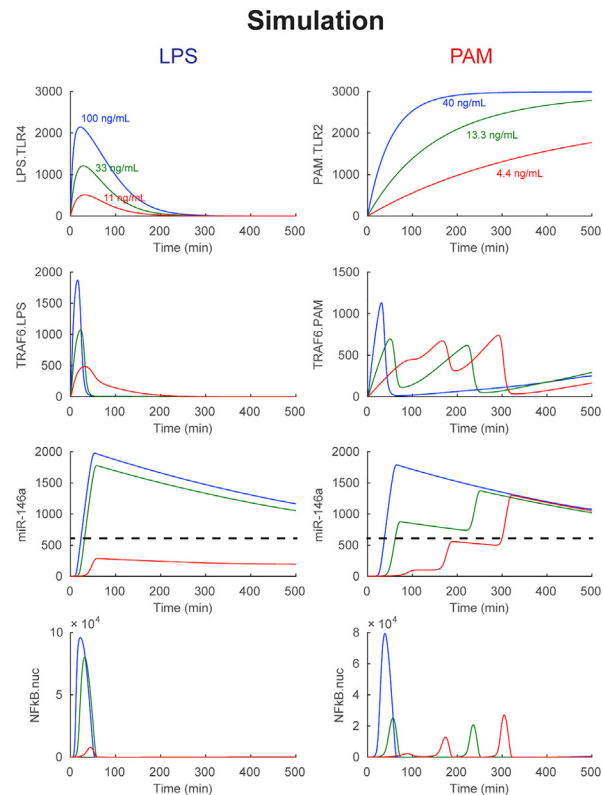
(B) Single-cell NF- κ B dynamic profiles of cells stimulated with PAM in microfluidic chambers, shown in line plots (upper row) and heatplots (lower row). Each row of the heatplot corresponds to one cell, with color indicating nuclear NF- κ B (green, low; red, high). PAM input leads to markedly different NF- κ B dynamics, with strong delay and increasing peak amplitude with decreasing dose (bolded line, example cell in each dose condition).

(C and D) Quantification of dynamic features of the LPS and PAM response. The horizontal and vertical bars represent median and interquartile range, respectively. (C) Comparison of response timing between LPS and PAM input. With decreasing dose, PAM first peak and maximum amplitude peak occur with greater delay compared to LPS response. In the case of LPS, the first peak is also the maximum peak in all cells. First peak amplitude and max peak time distinguish LPS and PAM responses. *Statistical significance with $p < 0.001$ by Mann-Whitney test. (D) Difference between NF- κ B peak first and maximum peak amplitude becomes more pronounced at lower PAM/LPS dose. LPS first peak response amplitude decreases significantly while PAM first peak amplitude decreases as well. LPS fraction of active cells decreased while PAM caused activation in essentially all cells in this dose range. At low/medium dose the LPS and PAM dynamics appear distinguished by the delay and rising nature of amplitude in the PAM response.

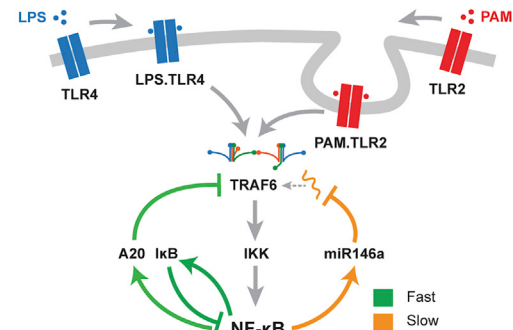
(E) To test the separability of the two responses, we applied a classification approach. A bagging classifier is an ensemble of decision tree models, where each decision-tree model determines whether a test trajectory is more similar to LPS-like or PAM-like. The bagging classifier classifies as LPS-like (PAM-like) response if most decision trees agree (with more than v fraction). Otherwise the bagging classifier outputs “Uncertain.”

(F) The two responses types are highly distinguishable based on classification, with >80% correctly assigned and the remainder uncertain.

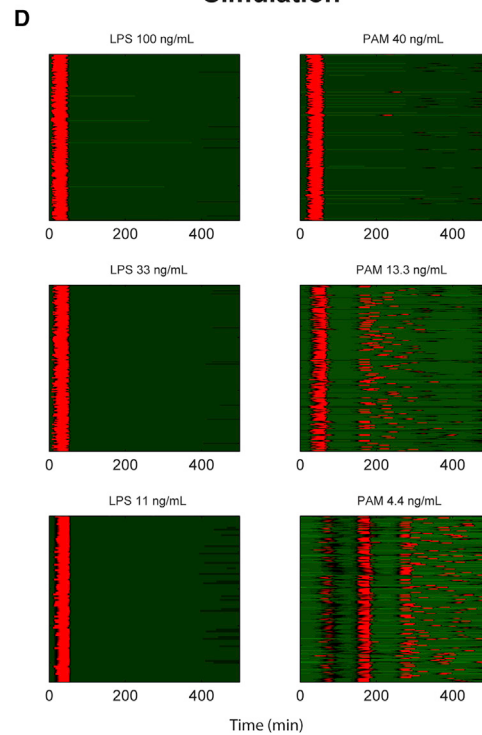
A



E

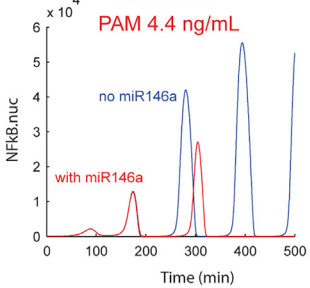


Simulation



B

Simulation



C

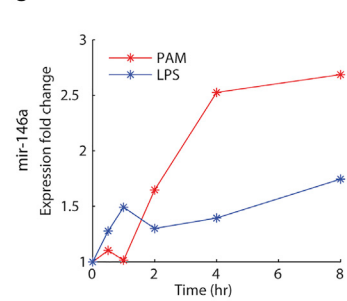


Figure 2. Receptor-Level Activation and Negative Feedback Dynamics Distinguish LPS versus PAM NF-κB Response

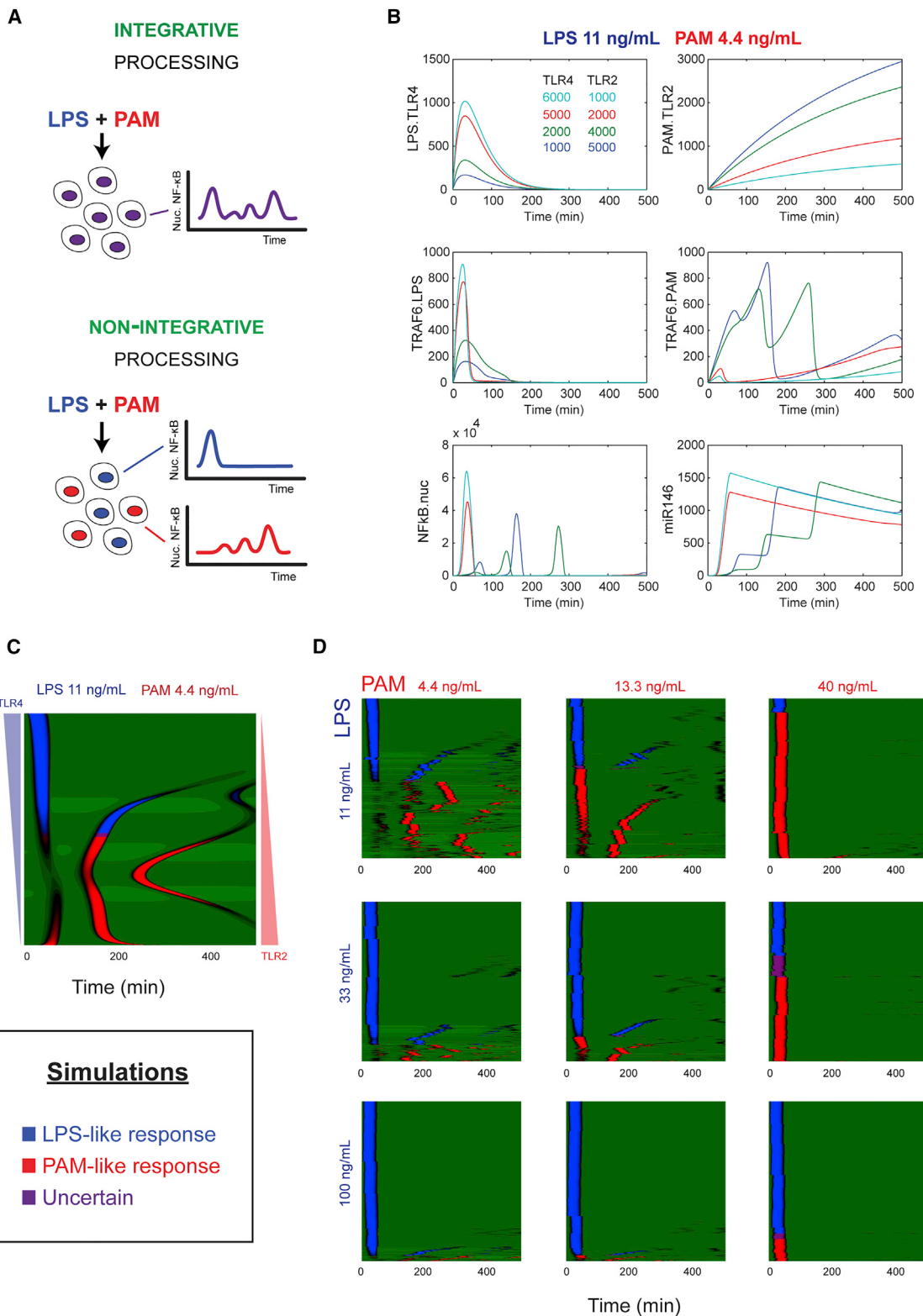
(A) NF-κB system dynamics for LPS and PAM at the experimentally tested doses. LPS bound to receptor (LPS.TLR4) complexes on the cell membrane under LPS activation lead to rapid TRAF6 induction and NF-κB activation. Under PAM stimulation, upstream endosomal signaling leads to rising accumulation of TRAF6 over time and increasing amplitude in the NF-κB response over time for low-dose PAM. Dashed line indicates the threshold level of miR-146a required to cause pathway inhibition.

(B) Simulations showed that low-dose PAM (4.4 ng/mL) caused an increasing amplitude response with rapid response shut-off at 300–400 min. We hypothesized that an unaccounted for negative feedback in the pathway could mediate this effect.

(C) Expression of miR-146a following 10 ng/mL LPS and 10 ng/mL PAM stimulation using a miR-146a TaqMan real-time PCR assay. Mir-146a is induced by both LPS and PAM stimulation, although with differing temporal profiles for the respective inputs. In contrast to rapid IκB/A20 feedback, mir-146a induction occurs on a slower timescale and maintains high expression.

(D) Heatplots of simulation cell populations for LPS and PAM inputs, showing good agreement with experimental data (Figures 1A and 1B). Only active cells are plotted in the heatmaps.

(E) NF-κB model schematic. TLR2 and TLR4 signal along the MyD88 pathway to activate TRAF6 and IKK. Clustering of TRAF6 and adaptor proteins leads to cooperative IKK induction. IKK activates NF-κB and negative feedback through IκB α , A20, and miR-146a. The TLR2 pathway requires endosomal processing for signal transduction, while TLR4 initiates signaling from the cell surface (Brandt et al., 2013; Stack et al., 2014). While IκB is the principal “fast” feedback, miR-146a mediates “slow” and ultrasensitive negative feedback that prevents continued growth of NF-κB oscillations under low-dose PAM input. PAM dose determines accumulation rate of PAM.TLR2 complexes.

**Figure 3. Relative TLR4-TLR2 Pathway Sensitivity Polarizes Single-Cell Response under Competing Ligands**

(A) Two possibilities for processing competing input signals. In integrative processing, cells exhibit dynamics that reflect the additive contribution of the two pathways (top). In non-integrative processing, cell response dynamics correspond to only one of the input signals.

(legend continued on next page)

Our initial model did not reproduce the abrupt shut off in TLR2-induced NF- κ B dynamics at ~300–400 min post-stimulus and instead showed continuing oscillations with growing peak height (Figure 2B). We hypothesized that the response shut off could be due to an unaccounted for negative feedback regulator. One possible candidate is miR-146a, which mediates a recently characterized additional negative feedback in the NF- κ B pathway acting to inhibit TRAF6 as a result of NF- κ B induction (Nahid et al., 2011, 2009; Quinn et al., 2013; Taganov et al., 2006). miR-146-mediated cleavage of TRAF6 mRNA leads to a rapid loss of TRAF6 protein and attenuated NF- κ B response (Nahid et al., 2009). To understand whether miR-146 is active in our cells and contributing to the rapid shut off in NF- κ B activity, we measured dynamic induction of this miRNA. We found that both PAM (10 ng/mL) and LPS (10 ng/mL) cause sustained upregulation of miR-146a (Figure 2C). Under LPS, miR-146a was induced starting from 1 hr and under PAM, at ~2 hr post-stimulus. Notably, rather than returning to baseline like I κ B and A20 negative feedback regulators, miR-146a maintained a high expression level for several hours (Figure 2C) (Gantier et al., 2011). The timescale of microRNA (miRNA) abundance corresponded with the timing in shutoff of the PAM response (Figure 1B, 2B-C). Incorporating miR-146a in the model as a slow-activating negative feedback, we recapitulated the NF- κ B response shutoff observed in experiments (Figures 2A and 2D). Modeling extrinsic noise in receptor levels reproduced experimental cell-to-cell variability in NF- κ B dynamics (Eldar and Elowitz, 2010; Elowitz et al., 2002) (Figures 1C, 1D, 2D, and S2).

TLR2- and TLR4-Polarized Responses under Co-stimulation in Single-Cell Simulations

Experiments showed that independent TLR4 and TLR2 stimulation induced distinct NF- κ B dynamics in single cells, and therefore we used NF- κ B dynamics as a lens for exploring how cells process simultaneous TLR inputs. Under TLR2 and TLR4 co-stimulation, the dynamic output could reflect features of both inputs (“integrative” processing), or alternatively the response could correspond to only one of the two inputs (“non-integrative” processing) (Figure 3A).

We reasoned that for multiple competing inputs to a digital pathway, the cell’s response could be influenced by sensitivity of the cell to each of the respective input signals. Intuitively, LPS attempts to active cells first due to delay by endosomal signaling of PAM/TLR2. In cells with high sensitivity to TLR4 ligands, LPS causes a rapid IKK/NF- κ B activation and an induction of transient (I κ B-mediated) and sustained (miRNA-mediated) negative feedback (Nahid et al., 2011, 2009; Taganov et al., 2006), preventing PAM signaling and allowing cells to only respond to the LPS signal. Meanwhile, in cells where TLR4 activation does not occur (high sensitivity to TLR2

ligands), PAM signaling can proceed and cells exhibit a PAM-like response.

To examine our reasoning, we used our model (Figure 2) to study simultaneous LPS-PAM input (Figure 3A). Simulation with low-dose LPS and low-dose PAM showed that cells with more sensitivity to TLR4 exhibit a single peak non-oscillatory response (characteristic of LPS input), and cells with more sensitivity to TLR2 exhibit a rising-amplitude, oscillatory response (characteristic of PAM input) (Figure 3B). We further simulated 500 cells with sensitivity shifting from TLR4 to TLR2 and applied our classifier to define these trajectories as LPS-like (blue), PAM-like (red), or mixed/uncertain (purple) responses (Figure 3C). This analysis revealed a highly sensitive transition from LPS-like to PAM-like response, indicating that cell response can be polarized to either LPS-like or PAM-like due to extrinsic noise.

Finally, to characterize how signal processing depends on relative dose of two input signals, we simulated NF- κ B responses for low, medium, and high LPS-PAM dose combinations. The proportion of cells exhibiting LPS-like (PAM-like) response increased with the relative dose of LPS (PAM) (Figure 3D), and cells exhibiting mixed responses remained in the minority for all dose combinations. Overall, these simulations suggested that cells employ a non-integrative processing mechanism for LPS-PAM co-stimulation.

Non-integrative Processing of Competing Inputs Leads to a Signaling Decision

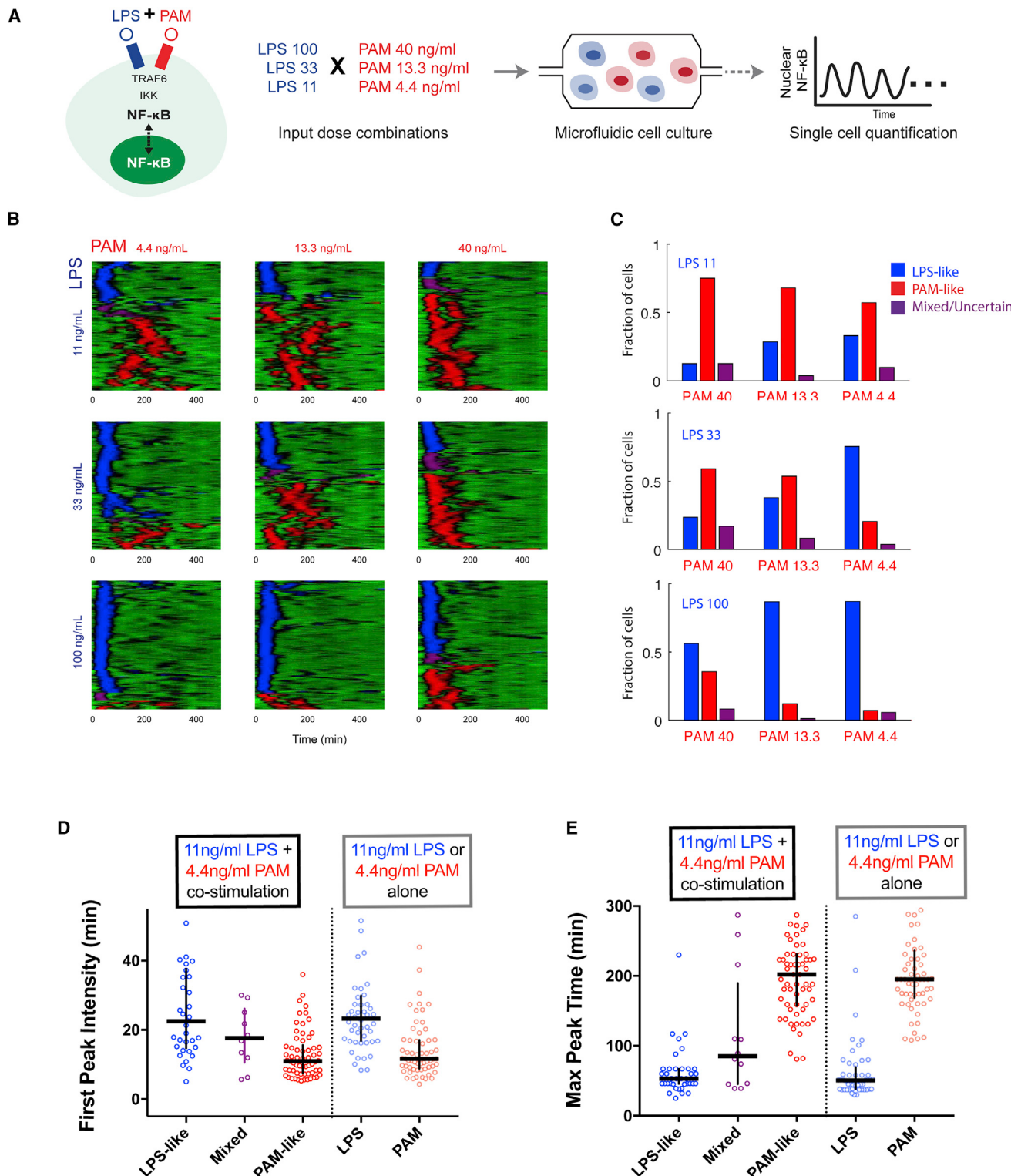
To experimentally test competing TLR stimulation, we delivered nine LPS-PAM dose combinations in microfluidic cell culture and monitored single-cell NF- κ B dynamics using live cell imaging (Figure 4A). We applied bagging classification to classify these traces into LPS-like, PAM-like, and mixed/uncertain classes (Figure 4B), and the fractions for each LPS-PAM dose combination were shown in Figure 4C. Consistent with model simulation, cells tended to show either an LPS-like or a PAM-like response. When both LPS and PAM were delivered at low dose (Figure 4B, upper left panel), LPS-like and PAM-like dynamic responses occurred most notably, and only 15% of cell responses were classified as “mixed/uncertain.” We also observed the dependency of response type on the input dose (Figure 4C) as found in the model (Figure 3D). For example, as LPS concentration decreased from high to low while maintaining low PAM dose, the fraction of cells showing LPS-like dynamics decreases from ~90% to ~40% of cells in the population (Figures 4B and 4C). These results provide experimental evidence of non-integrative processing of multiple simultaneous input signals.

We compared NF- κ B response characteristics for LPS-like and PAM-like classes and to NF- κ B dynamics induced by LPS and PAM stimulation alone. LPS and PAM show statistically distinct first peak intensity and maximum peak response time,

(B) Simulations of NF- κ B system response under simultaneous LPS/PAM input. As cells become relatively more sensitive for TLR4 or TLR2, the NF- κ B response displays a response characteristic of LPS or PAM, respectively.

(C) In simulations of cell populations with cell variability, applying the classifier trained on each input individually shows that the population partitions into those cells responding in an LPS-like fashion and PAM-like fashion, with few cells in the uncertain classification. In the panel, from top to bottom, the number of TLR4 is decreasing and the number of TLR2 is increasing.

(D) Under simulated co-stimulation with LPS and PAM, most cells respond in either LPS-like or PAM-like fashion, in correlation with the relative level of the two inputs.

**Figure 4. Experimentally Observed Non-integrative Processing of Simultaneous TLR Signals**

(A) Experimental scheme for testing competing LPS and PAM input signals. Using microfluidic cell culture, we deliver nine combinations of mixed LPS-PAM concentrations and record dynamic NF- κ B activation by live imaging.

(legend continued on next page)

and there is no significant difference in first peak intensity or maximum peak time between LPS-like (PAM-like) response classes compared to LPS (PAM) stimulation alone (**Figures 4D, 4E, and S4; Tables S8 and S9**). This analysis provides further support of distinct LPS- and PAM-like responses under co-stimulation.

Due to sustained negative feedback by candidate regulators such as mir-146a, we expected that cells activated by one input could show tolerance to another signal delivered several hours later. We tested this idea with a repeated stimulation strategy (**Figure 5A**): first an LPS stimulus, followed by a PAM stimulus 2 hr later to the same cells. Simulation indicated that a low-dose (11 ng/mL) LPS stimulus would activate approximately half of the cells in the population and the remaining cells would respond to a medium-dose PAM stimulus (13.3 ng/mL) 2 hr later (**Figure 5B**). Indeed, experiments found that 53% of cells responded to the first LPS stimulus and an additional 30% responded to the second PAM stimulus. Only 17% of cells responded to both stimuli, indicating that rapid negative feedback induced by the LPS signal is sufficient to inhibit a subsequent PAM response. Moreover, negative feedback induced by an initial medium-dose PAM signal was enough to fully block response to a high-dose LPS signal 4 hr later (**Figures 5A, 5B, and 5D**). Overall, these experiments show that variable sensitivity in the population combined with negative feedback mediates non-integrative processing and distinct LPS- and PAM-like responses under simultaneous LPS-PAM input (**Figure 5E**).

DISCUSSION

Cells interact in complex environments containing a multitude of signals. During infection, different pathogen-associated signals simultaneously transduce information through Toll-like receptors to the NF- κ B pathway. It has been unclear how a single signaling pathway handles multiple simultaneous inputs. NF- κ B activation is switch-like or digital in that a threshold input level must be exceeded to trigger pathway activation, and here we explored digital NF- κ B signaling downstream of simultaneous TLR2-TLR4 stimulation. When stimulated by LPS and PAM alone, TLR4 and TLR2 induce distinct NF- κ B dynamic profiles, consistent with previous findings that pathway dynamics encode ligand specificity (**Behar et al., 2013; Caldwell et al., 2014; Werner et al., 2005**). LPS and PAM both induce an inflammatory gene program, however, LPS additionally induces antiviral genes including *ifnb1* mediated by polo-like kinases such as *plk1* (**Amit et al., 2009; Chevrier et al., 2011**). Distinct regulation of antiviral responses occurs through mathematical modeling and experiments showed that simultaneous engagement of TLR4 and TLR2 caused polarized responses in the population with

single cells responding in “LPS-like” or “PAM-like” fashion rather than a combined or mixed fashion. This separation is clearest under low-dose stimulation where TLR2 and TLR4 NF- κ B dynamics are most distinct. We termed this type of response “non-integrative processing,” in contrast to “integrative processing” where single-cell dynamic response combines features of multiple inputs (**Figure 3A**). Because TLR4 and TLR2 pathways share downstream signaling components, non-integrative processing represents a “first to fire” modality for cells to achieve ligand-specific responses despite pathway crosstalk.

Switch-like activation in cell signaling is typically associated with decision robustness under noisy inputs (**Dueber et al., 2007; Kellogg et al., 2015**). Here, we illuminate an additional consequence of switch-like activation for simultaneous input signals called non-integrative processing. Understanding how cells manage multiple inputs and integrate signals is a core problem essential for understanding cell behavior in real signaling contexts. Cell-to-cell variability, an inevitable attribute of cell populations, determines whether a cell responds to LPS or to PAM (**Figure 5**). TLR2 and TLR4 have specific roles in processing gram-positive and gram-negative bacteria, respectively, with distinct gene expression and cytokine profiles (**Hirata et al., 2008; Takeuchi et al., 1999**). Subsets of the cell population responding to specific signals may underlie cell-cell cooperation in combating infection (**Trinchieri and Sher, 2007**). Simultaneous engagement of TLR4 and TLR2 was shown to synergistically activate production of cytokines including TNF and IL-12, through paracrine interactions including IFN signaling (**Beutler et al., 2001; Sato et al., 2000**). Moreover, inhibitory cell-cell interactions were observed including inhibition of TLR4-induced Th1 cytokines by IL-10 produced through TLR2 (**Re and Strominger, 2004**). Therefore, heterogeneous and polarized responses at the single-cell level may mediate inter-cellular communication in the innate immune tissue response.

EXPERIMENTAL PROCEDURES

Cell Lines

Mouse (3T3) fibroblasts expressing near-endogenous p65 levels were described previously (**Tay et al., 2010**). Briefly, p65^{-/-} mouse 3T3 fibroblasts were engineered to express p65-DsRed under control of 1.5 kb p65 promoter sequence (**Lee et al., 2009; Tay et al., 2010**). The cell line was clonally derived to express the p65 subunit of NF- κ B fused to a fluorescent protein (p65-DsRed) at lowest detectable level to preserve near endogenous expression (**Lee et al., 2009**). Addition of ubiquitin-promoter-driven H2B-GFP expression provided a nuclear label to facilitate automated tracking and image processing.

Automated Microfluidic Cell Culture System

Automated microfluidic cell culture was performed as previously described (**Tay et al., 2010**). Briefly, microfluidic chambers were fibronectin-treated and seeded with cells at ~200 cells/chamber. Standard culture conditions of

(B) Single-cell traces under combined inputs displayed in heatmap form with single-cell temporal trajectories displayed in horizontal lines. The class of each response is colored blue for LPS-like, red for PAM-like, and purple for mixed/uncertain. We observe a low occurrence of mixed responses and single-cell responses tend to belong to either LPS or PAM classes.

(C) Comparison of the proportion of cells showing LPS-like, PAM-like, and uncertain responses for each LPS-PAM input. The proportion of cells showing LPS-like response increases with relatively greater LPS concentration while more cells respond in PAM-like with relatively greater PAM concentration.

(D and E) Comparison of LPS-like (PAM-like) classes under co-stimulation to LPS (PAM) stimulation alone. LPS-like and PAM-like classes differ significantly in both first peak intensity (D) and max peak time (E) ($p < 0.0001$ by Mann-Whitney test). Furthermore, no significant difference exists between LPS-like (PAM-like) class under co-stimulation versus PAM (LPS) stimulation alone (**Table S9**). Horizontal line, median; vertical line, interquartile range.

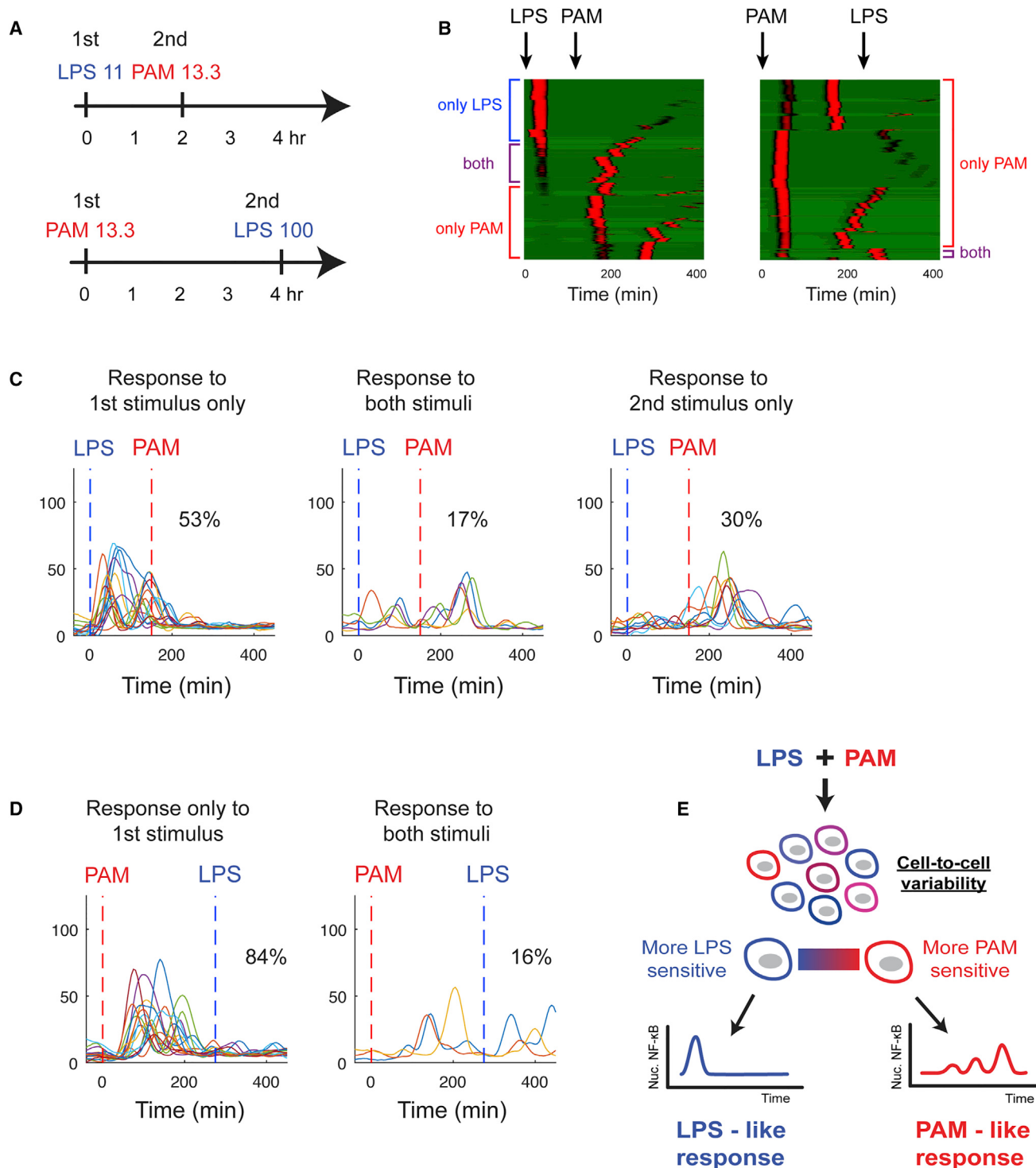


Figure 5. Cell Variability Underlies Non-integrative Processing

(A) Experimental scheme for sequential LPS/PAM stimulation. In the first experiment, LPS is provided first followed by PAM stimulus 2 hr later. In the second experiment, PAM is provided first followed by LPS 4 hr later.

(B) Model simulation of providing a LPS stimulus followed by a PAM stimulus, showing that those cells not responding to the first LPS signal subsequently do respond to the PAM signal (left). Conversely applying a moderate PAM stimulus first is sufficient to fully block LPS responses (right). Because the data are for sequential stimulations, responses are not classified as LPS- or PAM-like and shown in uniform color.

(legend continued on next page)

5% CO₂ and 37°C were maintained using an incubation chamber. Cells were allowed to grow for 1 day with periodic media replenishment until 80% confluence. Because some LPS preparations can activate both TLR4 and TLR2, we used a purified LPS preparation known to exclusively activate TLR4 signaling (Fujihara et al., 2003; Lee et al., 2009). Ultrapure LPS (Invivogen) and PAM (Invivogen) were diluted in DMEM media in vials pressured with 5% CO₂ and kept on ice. To stimulate cells, media equilibrated to 5% CO₂ and containing the desired LPS or PAM amount was delivered to chambers, leading to a step increase in LPS concentration. All LPS and PAM doses were tested in parallel in a single chip. Stimulations were applied in duplicate chambers on the chip. Following stimulation, chambers were sealed and imaged at 5- to 6-min intervals.

Image Acquisition and Data Analysis

DsRed and GFP channels were acquired using a Leica DMI6000B wide field microscope at 20× magnification with a Retiga-SRV CCD camera (QImaging) using Leica L5 and Y3 filters to acquire GFP and DsRED signals, respectively, and a Leica EL6000 mercury metal halide light source. CellProfiler software (<http://cellprofiler.org/>) and custom MATLAB software was used to automatically track cells and quantify NF-κB translocation, and automated results were manually compared with images to ensure accuracy prior to further analysis. NF-κB activation was quantified as mean nuclear fluorescence intensity normalized by mean cytoplasm intensity. For peak analysis, data were smoothed (MATLAB function smooth) followed by peak detection (MATLAB function mspeaks) to extract NF-κB peak properties (intensity, area, delay) with manual verification using a custom interface in MATLAB. Statistical analysis of NF-κB peak amplitude and timing data was performed by Mann-Whitney test (Graphpad Prism). Heatplots of single cell traces are sorted by Pearson correlation coefficient similarity.

miRNA Gene Expression Analysis

For miRNA expression time course following challenge, total RNA was isolated with the mirVana miRNA isolation kit (Ambion). cDNA was generated using the TaqMan microRNA reverse transcription kit (Applied Biosystems). Relative expression of miRNA was determined using TaqMan miRNA-specific assay *hsa-miR-146a* specific for both human and murine miR-146a, and expression was normalized using *snoRNA234* small nuclear RNA (snRNA) endogenous control probes (Applied Biosystems).

Bagging Classifier

For LPS dose x and PAM dose y , we trained a bagging classifier with NF-κB time courses stimulated by either LPS (dose x , denoted as LPS-like) or PAM (dose y , denoted as PAM-like). The bagging classifier is an ensemble of N decision tree models, where the training data for each decision tree was generated by bootstrapping. Given one NF-κB time course induced by two stimuli, we obtain the prediction of every decision tree model. If most predictions (more than v , $v > 0.5$) classify the time course as LPS-like (PAM-like), the bagging classifier outputs LPS-like (PAM-like). Otherwise, the bagging classifier outputs uncertain. The classifier was implemented using MATLAB function fitensemble with arguments “Bag,” “Tree,” and “Classification.” Details of the construction of the classifiers and selection of parameter values can be found in the [Supplemental Experimental Procedures](#).

SUPPLEMENTAL INFORMATION

Supplemental Information includes Supplemental Experimental Procedures, four figures, and nine tables and can be found with this article online at <http://dx.doi.org/10.1016/j.celrep.2017.03.027>.

- (C) Experimental data for LPS-first stimulation: 53% of cells respond only to the LPS input, 17% respond to both the first and second stimulus, and 30% respond to only the second stimulus.
- (D) Experiment where PAM stimulus is provided first, followed by LPS 4 hr later. PAM 13.3 input activated all cells, and only 16% of cells were able to respond to a strong LPS signal at 4 hr.
- (E) Overall findings: simultaneous LPS and PAM input leads to non-integrative processing at the population level. In responding to a mixed LPS-PAM input, cells respond in either an LPS-like or PAM-like dynamic fashion. Cells in the population have variable sensitivity for LPS and PAM inputs. Cells that are relatively more sensitive to PAM respond in a PAM-like fashion to competing LPS-PAM input. The converse is true for cells relatively more sensitive to LPS.

AUTHOR CONTRIBUTIONS

R.A.K., S.T., and M.E. performed experiments. R.A.K., C.T., and M.E. analyzed experiments. C.T. constructed the mathematical model. R.A.K. drafted the manuscript. All authors revised and edited the manuscript. S.T. supervised the project.

ACKNOWLEDGMENTS

We acknowledge Namiko Mitarai for fruitful discussion. This work was supported by an ERC Starting Grant (SingleCellDynamics) and an NIH grant (R01 GM117134-01) to S.T. and by Danish National Research Foundation (Center for Models of Life) to C.T.

Received: October 20, 2016

Revised: January 11, 2017

Accepted: March 6, 2017

Published: April 4, 2017

REFERENCES

- Akira, S., and Takeda, K. (2004). Toll-like receptor signalling. *Nat. Rev. Immunol.* 4, 499–511.
- Amit, I., Garber, M., Chevrier, N., Leite, A.P., Donner, Y., Eisenhaure, T., Guttman, M., Grenier, J.K., Li, W., Zuk, O., et al. (2009). Unbiased reconstruction of a mammalian transcriptional network mediating pathogen responses. *Science* 326, 257–263.
- Behar, M., Barken, D., Werner, S.L., and Hoffmann, A. (2013). The dynamics of signaling as a pharmacological target. *Cell* 155, 448–461.
- Beutler, E., Gelbart, T., and West, C. (2001). Synergy between TLR2 and TLR4: a safety mechanism. *Blood Cells Mol. Dis.* 27, 728–730.
- Brandt, K.J., Fickentscher, C., Kruthof, E.K.O., and de Moerloose, P. (2013). TLR2 ligands induce NF-κB activation from endosomal compartments of human monocytes. *PLoS ONE* 8, e80743.
- Caldwell, A.B., Cheng, Z., Vargas, J.D., Birnbaum, H.A., and Hoffmann, A. (2014). Network dynamics determine the autocrine and paracrine signaling functions of TNF. *Genes Dev.* 28, 2120–2133.
- Cheong, R., Rhee, A., Wang, C.J., Nemenman, I., and Levchenko, A. (2011). Information transduction capacity of noisy biochemical signaling networks. *Science* 334, 354–358.
- Chevrier, N., Mertins, P., Artyomov, M.N., Shalek, A.K., Iannaccone, M., Caciocia, M.F., Gat-Viks, I., Tonti, E., DeGrace, M.M., Clouser, K.R., et al. (2011). Systematic discovery of TLR signaling components delineates viral-sensing circuits. *Cell* 147, 853–867.
- Dietrich, N., Lieneklaus, S., Weiss, S., and Gekara, N.O. (2010). Murine toll-like receptor 2 activation induces type I interferon responses from endosomal compartments. *PLoS ONE* 5, e10250.
- Dietterich, T.G. (2000). An experimental comparison of three methods for constructing ensembles of decision trees. *Mach. Learn.* 40, 139–157.
- Dueber, J.E., Mirsky, E.A., and Lim, W.A. (2007). Engineering synthetic signaling proteins with ultrasensitive input/output control. *Nat. Biotechnol.* 25, 660–662.
- Eldar, A., and Elowitz, M.B. (2010). Functional roles for noise in genetic circuits. *Nature* 467, 167–173.

- Elowitz, M.B., Levine, A.J., Siggia, E.D., and Swain, P.S. (2002). Stochastic gene expression in a single cell. *Science* 297, 1183–1186.
- Ferrell, J.E., and Machleder, E.M. (1998). The biochemical basis of an all-or-none cell fate switch in *Xenopus* oocytes. *Science* 280, 895–899.
- Fujihara, M., Muroi, M., Tanamoto, K., Suzuki, T., Azuma, H., and Ikeda, H. (2003). Molecular mechanisms of macrophage activation and deactivation by lipopolysaccharide: roles of the receptor complex. *Pharmacol. Ther.* 100, 171–194.
- Gantier, M.P., McCoy, C.E., Rusinova, I., Saulep, D., Wang, D., Xu, D., Irving, A.T., Behlke, M.A., Hertzog, P.J., Mackay, F., and Williams, B.R.G. (2011). Analysis of microRNA turnover in mammalian cells following Dicer1 ablation. *Nucleic Acids Res.* 39, 5692–5703.
- Gómez-Sjöberg, R., Leyrat, A.A., Pirone, D.M., Chen, C.S., and Quake, S.R. (2007). Versatile, fully automated, microfluidic cell culture system. *Anal. Chem.* 79, 8557–8563.
- Hirata, N., Yanagawa, Y., Ebihara, T., Seya, T., Uematsu, S., Akira, S., Hayashi, F., Iwabuchi, K., and Onoé, K. (2008). Selective synergy in anti-inflammatory cytokine production upon cooperated signaling via TLR4 and TLR2 in murine conventional dendritic cells. *Mol. Immunol.* 45, 2734–2742.
- Hoffmann, A., Levchenko, A., Scott, M.L., and Baltimore, D. (2002). The IkappaB-NF-kappaB signaling module: temporal control and selective gene activation. *Science* 298, 1241–1245.
- Kellogg, R.A., and Tay, S. (2015). Noise facilitates transcriptional control under dynamic inputs. *Cell* 160, 381–392.
- Kellogg, R.A., Gómez-Sjöberg, R., Leyrat, A.A., and Tay, S. (2014). High-throughput microfluidic single-cell analysis pipeline for studies of signaling dynamics. *Nat. Protoc.* 9, 1713–1726.
- Kellogg, R.A., Tian, C., Lipniacki, T., Quake, S.R., and Tay, S. (2015). Digital signaling decouples activation probability and population heterogeneity. *eLife* 4, e08931.
- Kingeter, L.M., Paul, S., Maynard, S.K., Cartwright, N.G., and Schaefer, B.C. (2010). Cutting edge: TCR ligation triggers digital activation of NF-kappaB. *J. Immunol.* 185, 4520–4524.
- Kopp, E., and Medzhitov, R. (2003). Recognition of microbial infection by Toll-like receptors. *Curr. Opin. Immunol.* 15, 396–401.
- Lee, T.K., Denny, E.M., Sanghvi, J.C., Gaston, J.E., Maynard, N.D., Hughey, J.J., and Covert, M.W. (2009). A noisy paracrine signal determines the cellular NF-kappaB response to lipopolysaccharide. *Sci. Signal.* 2, ra65.
- Liu, T., Yamaguchi, Y., Shirasaki, Y., Shikada, K., Yamagishi, M., Hoshino, K., Kaisho, T., Takemoto, K., Suzuki, T., Kuranaga, E., et al. (2014). Single-cell imaging of caspase-1 dynamics reveals an all-or-none inflammasome signaling response. *Cell Rep.* 8, 974–982.
- Malleshaiah, M.K., Shahrezaei, V., Swain, P.S., and Michnick, S.W. (2010). The scaffold protein Ste5 directly controls a switch-like mating decision in yeast. *Nature* 465, 101–105.
- Nahid, M.A., Pauley, K.M., Satoh, M., and Chan, E.K.L. (2009). miR-146a is critical for endotoxin-induced tolerance: implication in innate immunity. *J. Biol. Chem.* 284, 34590–34599.
- Nahid, M.A., Satoh, M., and Chan, E.K. (2011). MicroRNA in TLR signaling and endotoxin tolerance. *Cell. Mol. Immunol.* 8, 388–403.
- Ozinsky, A., Underhill, D.M., Fontenot, J.D., Hajjar, A.M., Smith, K.D., Wilson, C.B., Schroeder, L., and Aderem, A. (2000). The repertoire for pattern recognition of pathogens by the innate immune system is defined by cooperation between toll-like receptors. *Proc. Natl. Acad. Sci. USA* 97, 13766–13771.
- Philpott, D.J., and Girardin, S.E. (2004). The role of Toll-like receptors and Nod proteins in bacterial infection. *Mol. Immunol.* 41, 1099–1108.
- Quinn, E.M., Wang, J.H., O'Callaghan, G., and Redmond, H.P. (2013). MicroRNA-146a is upregulated by and negatively regulates TLR2 signaling. *PLoS ONE* 8, e62232.
- Re, F., and Strominger, J.L. (2004). IL-10 released by concomitant TLR2 stimulation blocks the induction of a subset of Th1 cytokines that are specifically induced by TLR4 or TLR3 in human dendritic cells. *J. Immunol.* 173, 7548–7555.
- Sato, S., Nomura, F., Kawai, T., Takeuchi, O., Mühlradt, P.F., Takeda, K., and Akira, S. (2000). Synergy and cross-tolerance between toll-like receptor (TLR) 2- and TLR4-mediated signaling pathways. *J. Immunol.* 165, 7096–7101.
- Selimkhanov, J., Taylor, B., Yao, J., Pilko, A., Albeck, J., Hoffmann, A., Tsimring, L., and Wollman, R. (2014). Accurate information transmission through dynamic biochemical signaling networks. *Science* 346, 1370–1373.
- Shah, N.A., and Sarkar, C.A. (2011). Robust network topologies for generating switch-like cellular responses. *PLoS Comput. Biol.* 7, e1002085.
- Shinohara, H., Behar, M., Inoue, K., Hiroshima, M., Yasuda, T., Nagashima, T., Kimura, S., Sanjo, H., Maeda, S., Yumoto, N., et al. (2014). Positive feedback within a kinase signaling complex functions as a switch mechanism for NF- κ B activation. *Science* 344, 760–764.
- Simmons, D.P., Canaday, D.H., Liu, Y., Li, Q., Huang, A., Boom, W.H., and Harding, C.V. (2010). Mycobacterium tuberculosis and TLR2 agonists inhibit induction of type I IFN and class I MHC antigen cross processing by TLR9. *J. Immunol.* 185, 2405–2415.
- Stack, J., Doyle, S.L., Connolly, D.J., Reinert, L.S., O'Keeffe, K.M., McLoughlin, R.M., Paludan, S.R., and Bowie, A.G. (2014). TRAM is required for TLR2 endosomal signaling to type I IFN induction. *J. Immunol.* 193, 6090–6102.
- Taganov, K.D., Boldin, M.P., Chang, K.-J., and Baltimore, D. (2006). NF-kappaB-dependent induction of microRNA miR-146, an inhibitor targeted to signaling proteins of innate immune responses. *Proc. Natl. Acad. Sci. USA* 103, 12481–12486.
- Takeda, K., and Akira, S. (2005). Toll-like receptors in innate immunity. *Int. Immunopharmacol.* 17, 1–14.
- Takeuchi, O., Hoshino, K., Kawai, T., Sanjo, H., Takada, H., Ogawa, T., Takeda, K., and Akira, S. (1999). Differential roles of TLR2 and TLR4 in recognition of gram-negative and gram-positive bacterial cell wall components. *Immunity* 11, 443–451.
- Tay, S., Hughey, J.J., Lee, T.K., Lipniacki, T., Quake, S.R., and Covert, M.W. (2010). Single-cell NF-kappaB dynamics reveal digital activation and analogue information processing. *Nature* 466, 267–271.
- Trinchieri, G., and Sher, A. (2007). Cooperation of Toll-like receptor signals in innate immune defence. *Nat. Rev. Immunol.* 7, 179–190.
- Werner, S.L., Barken, D., and Hoffmann, A. (2005). Stimulus specificity of gene expression programs determined by temporal control of IKK activity. *Science* 309, 1857–1861.

Supplemental Information

Cellular Decision Making

by Non-Integrative Processing of TLR Inputs

Ryan A. Kellogg, Chengzhe Tian, Martin Etzrodt, and Savaş Tay

1. Classifier

Description of Classifiers

We construct one classifier for every input condition, and the primary objective of this classifier is to determine whether a cellular response under co-stimulation is a more LPS-like, PAM-like or mixed response (if exist). For the input condition of LPS dose x and PAM dose y , the training data for the classifier are the time series of nuclear NF- κ B concentrations under only LPS dose x challenge or only PAM dose y challenge, and the test data are the time series under LPS dose x and PAM dose y co-stimulation. We obtain around 100-200 cellular responses from the experiments, and we only use active trajectories for training and testing. Our experiments show that the fractions of active cells are 95% for LPS 100 ng/mL, 73% for LPS 33 ng/mL, 47% for LPS 11 ng/mL and 100% for all other inputs. The size of training data therefore varies between 100 and 300 cells and the size of test data is around 100-200 for all input conditions. For classification of model-simulated time courses, the training data consist of at most 500 LPS-type (only active time courses are considered) and 500 PAM-type and the size of the test data is 500.

To determine the potential mixed-response, we employ a two-step procedure for classification. The first step is to construct individual classifiers to classify a test cellular response into more LPS-like or more PAM-like. We use bootstrap to diversify the training data for individual classifiers. The second step is to aggregate all outputs from the individual classifiers based on majority-vote: if more than v fraction of outputs gives LPS-like (PAM-like), we claim the test data is LPS-like (PAM-like); if the fraction of neither LPS outputs nor PAM outputs reaches v , this test data is considered uncertain and we interpret this data as the mixed type.

We notice that constructing individual classifiers based on explicit features could limit the performance in identifying mixed responses. The reason is that classifiers trained on explicit features will only evaluate the test data from pre-defined perspectives, and these perspectives may contain a bias on one of the two labels. To eliminate bias, we choose to employ a data-driven approach and allow classification algorithms to automatically determine the features that show the best separation of training data. In this work we use decision tree models to achieve this objective. A decision tree model contains many splits and each split represents a YES-NO question, and the classification outcome is determined by the answers to a series of YES-NO questions. The splits are determined by the algorithm such that the labels of resulting two groups (those answering YES and those answering NO) are as homogeneous as possible (minimizing Gini index). Due to the bootstrapping feature, we allow the decision trees to evaluate the test data from diverse perspectives. By definition, our classifier belongs to a bagging classifier.

One limitation of our data-driven approach is that some splits in the individual decision tree models may be induced by the noise in the data, rather than the difference between the LPS- and PAM-like cellular responses. These decision trees may give wrong classification results and individual decision tree models may not achieve a high level of agreement on apparent LPS- or PAM-like test data. Consequently, we should not choose the value of the threshold v to be very high. In principle, we may increase the value of v by increasing the size of the training data.

Selection of Parameters

We evaluate our classifier by cross-validation and we choose the values of two unknown parameters (number of decision trees N and the threshold v) by maximizing the accuracy. To be precise, for each combination of N and v , we train a bagging classifier for every input condition and compute the fractions that the classifier outputs a correct label (“correct”), an incorrect label (“incorrect”) or an uncertain label (“uncertain”) by 10-fold cross-validation. The overall accuracy of classifiers with (N, v) is defined as the average value of the “correct” fractions of all nine input conditions.

We sample the values of N and v in a wide range and the accuracies are shown in Table S1. We observe that the accuracy of the bagging classifiers is not strongly affected by the number of decision trees (N) except for very high thresholds (v), and that the accuracy decreases as the threshold values (v) increases. We then choose $N=50$ and restrict our attention to the input condition of our primary interest (LPS 11 ng/mL, PAM 4.4 ng/mL). We find that the primary cause for the reduction in the accuracy of the bagging classifier with higher v is the uncertain labels (Figure S1A), and this finding holds for all other input conditions (Figure S1B).

Based on the parameter sampling, we choose $N=50$, $v=0.6$ to be the optimal parameter values. We notice that $v=0.6$ also maximizes the fraction of incorrect labels, though this fraction is small. The resulting classifier has an average accuracy of 89% and an accuracy of at least 85% for every input condition (Table S1 and S2).

Example Decision Tree

An example decision tree for LPS 11 ng/mL and 4.4 ng/mL and its relevant statistics are shown in Figure S1C and Table S3. The importance is defined as the increase in node purity (how uniform the labels are) after split, and is computed with matlab command predictorImportance. The first two predictors of the tree, c(181) and c(228), evaluate the nuclear NF- κ B activities around 3 and 4 hours after stimulation. The decision tree is likely to classify trajectories with high values as PAM responses. The last two predictors, c(50) and c(16), evaluate the early NF- κ B activities and trajectories with high values are classified as LPS responses. This decision tree is consistent with the fact that LPS induces a rapid, short response while PAM induces a delayed but sustained response.

Classification with Threshold $v=0.8$

To further justify our choice for parameter values, we train classifiers with parameter values $N=50$, $v=0.8$ and repeat the classification figures in the main text (Figure 3D, Figure 4B-C), as shown in Figure S1F-G. We restrict our attention to mid/low doses of LPS and PAM to allow a sufficient difference between LPS-like and PAM-like responses. We show that no more than 10% of simulated cellular responses are determined to be mixed type (Figure S1F). For experimental cellular responses, our classifier predicts a substantially higher percentage of mixed type responses (20%-30%). Despite these high numbers, we argue that our main conclusion that cells process competing TLR ligands in a non-integrative

fashion still holds. Firstly, the percentage 20%-30% is still well below 50%, indicating that the majority of responses are still either LPS- or PAM-like. Secondly, the accuracy of the bagging classifier with $v=0.8$ is lower compared with the ones with lower threshold values. Figure S1B shows that when applied to training data, the classifier with $v=0.8$ outputs around 20% of mixed output, and we should take this number into account when interpreting the percentages in Figure S1G. Here we consider the differences between the percentages in Figure S1G (classifier's outputs for the test data) and 20% (classifier's outputs for the training data) to be a more realistic description of the actual percentage of mixed-type responses, which are around 10%, indicating that the mixed responses are a minority. In summary, we claim that our main conclusion is unaffected with a higher value of threshold v .

Classification of artificially generated “mixed” time courses

To evaluate the quality of our classifier in identification of mixed responses, we restrict to the low doses and create 1000 artificial “mixed” time courses by adding one randomly selected LPS-training trajectory and one randomly selected PAM-training trajectory. We then apply our classifier to these artificial data and plot the result in Figure S1D-E. Indeed, most artificial data are classified as mixed. If these artificial trajectories accurately reflect the reality, this analysis suggests that our classifier fails to identify around 40% mixed responses for this dose combination. The corrected fraction of mixed responses should be 10% (reported by classifier) divided by 60%, which equals to 16%. This is still a small number and we claim that our conclusion remains valid.

2. Mathematical Model of Competing TLR Ligands

We construct a mathematical model for competing TLR ligands by extending our previously published models of TNF and LPS pathways (Kellogg et al., 2015, Tay et al., 2010). All reactions are modeled using the mass action law. Activation and inactivation are modeled using Michaelis-Menten terms or Hill terms, if cooperativity exists. In this work, rather than fitting to experimental cellular responses precisely, our emphasis is to use mathematical models to illustrate the possibility that an ultrasensitive negative feedback and endosomal signaling can mediate non-integrative processing of competing ligands, and our model only needs to capture the main features of LPS and PAM cellular responses. For this reason, we put strong constraints to our models. We assume that the overall signaling network topology for both TLR4- and TLR2-mediated signaling is identical, and that the parameter values below TRAF6 are identical for both signaling pathways. This allows us to treat distinct signal inputs with reduced model complexity and to attribute the differences between the two pathways to the receptor-level parameter values. We also exclude intrinsic noises and only consider receptor-level extrinsic noise (total number of TLR4 and TLR2 follow lognormal distributions), so our simulated cellular responses are expected to be more “ordered” than the experiments.

Conversion from Concentration to Molecular Numbers

The microfluidics platform utilized in this study contains chambers of size 1.12 mm*0.9 mm*0.040 mm (Kellogg et al., 2014, Gómez-Sjöberg et al., 2007) and each chamber contains around 100 cells. The molecular weight of LPS is set to

10kDa (Sigma-Aldrich, 2008) and the molecular weight of Pam₃CSK₄ is 1509.6 Da (Invivogen). We then conclude that 1 ng/mL LPS input gives that every cell interacts with 2.4*10⁴ ligands, and 1 ng/mL PAM input gives 1.6*10⁵ ligands per cell.

Structure of the ODE Model

Table S4 summarizes the reactions and the mathematical descriptions for the receptor-level signaling. Here we assume that the total number of TLR4 (both in TLR4 and LPS.TLR4 forms) follows a log-normal distribution with parameter μ_l and σ_l , and the total number of TLR2 (both TLR2 and PAM.TLR2) follows a log-normal distribution with parameter μ_p and σ_p . LPS.TLR4 and PAM.TLR2 complexes function in distinct locations (Brandt et al., 2013). To account for this, we model TRAF6 molecules activated by LPS (denoted as TRAF6a(LPS)) and the ones activated by PAM (denoted as TRAF6a(PAM)) separately. Both forms of TRAF6a may activate IKK independently, and we model the reaction of IKK activation ($IKKn \rightarrow IKKa$) with rate

$$c_{1(LPS)} \frac{[TRAF6a(LPS)]^4}{[TRAF6a(LPS)]^4 + K_{TRAF6a(LPS)}^4} [IKKn] + c_{1(PAM)} \frac{[TRAF6a(PAM)]^4}{[TRAF6a(PAM)]^4 + K_{TRAF6a(PAM)}^4} [IKKn].$$

We integrate the transcriptional control of miR-146a in the same fashion as other transcripts, also shown in Table S4.

Parameter Values

To constrain the degrees of freedom in parameter estimation, we adopt the parameter values in TLR4-mediated receptor-level signaling from our previous LPS model (Kellogg et al., 2015), and we only adjust the binding rate between TLR4 and LPS to account for the lower fraction of active cells under ultrapure LPS challenge. We also assume that similar reactions in TLR4- and TLR2 signaling take the same kinetic constants whenever possible. The parameters related to miR-146a are obtained by fitting to the bulk expression data. The parameter values for the receptor-level signaling and the miR-146a are listed in Table S5.

Remarks

- Since our model is not designed to fit to experimental data precisely, we determine the parameter values by manual trial-and-error to avoid the computationally expensive process of parameter estimation.
- We exclude the TRIF-mediated TLR4 pathway from the model as we find that pure LPS has a high degradation rate in the experiments and few NF-κB responses are observed beyond the initial peak. This finding is supported by our previous work that an LPS stimulus without continuous perfusion yields cellular responses mainly with only one peak while a stimulus with perfusion yields sustained oscillation (Kellogg et al., 2015). Moreover, the TRIF pathway is not active in 3T3 cells (Alexander Hoffmann, personal correspondence).
- The mathematical model suggests that the non-integrative processing of LPS and PAM input signals can be explained by the different timescales in receptor-level signaling and the miR-146a negative feedback.

- The endosomal signaling of TLR2 is described by the receptor-level kinetic constants. The low binding rate between PAM and TLR2 (p_b) accounts for both binding and internalization processes. The low unbinding rate (p_f) models internalization as an integrator and allows the endosomal level of PAM.TLR2 to be less sensitive to the degradation of PAM input signal.
- To control the complexity of the model, we model the synthesis and degradation of miR-146a in a similar fashion to our TNF model (Tay et al., 2010). The activation rate of nuclear NF- κ B on miR-146a genes is slower than the rates for other genes. This is consistent with miR-146a functioning as a slow feedback (Figure 2).
- miR-146a inhibits signaling by targeting IRAK1/2 and TRAF6 mRNA (Nahid et al., 2011). Here we employ a phenomenological approach by modeling with a Hill term. The Hill coefficient 4 is chosen to account for the ultrasensitivity of the miR-146a negative feedback and can in principle be replaced by other integers greater than 1.
- We notice that the model requires a lower level of TRAF6a ($\sim 10^3$) than the Hill constant (k_{TRAF6a} , 3.5×10^3) to activate the downstream pathway. The reason is that we assume many parameter values to be identical to the LPS model where this Hill constant does not serve as the threshold due to the NF- κ B-level variability. It is worth mentioning that the predictive power of the model is not sacrificed as the cooperativity among TRAF6 in activating IKK is more relevant to digital signaling.
- The model predicts that LPS degradation inhibits NF- κ B oscillation after the first peak, without the necessity of miR-146a. This prediction is due to the fact that we use the relevant parameter values from the existing LPS model where miR-146a was not considered. One alternative possibility is that LPS degrades slower and the inhibition of NF- κ B oscillation was induced by miR-146a. However, the model maintains its predictive power since LPS activates the cell in a faster timescale than PAM.
- For PAM responses, our model predicts a stronger dependency of the maximal peak amplitudes on the input doses (Figure 1C and S2e). The reason is that we model endosomal signaling of PAM with the mathematical structure of membrane signaling, in order to eliminate several reactions and free parameters (Table S4). Consequently, the endosomal level of PAM.TLR2 complexes reaches the steady state value exponentially in time (Figure 2A). The rate of exponential accumulation and the steady state value are governed by the timescales of low-dose responses (~ 200 min delay and shut-off at 300-400 min), leaving us little flexibility to tune the dependency of the steady state value (governing the maximal peak amplitude) on the input dose. This issue can be possibly resolved by modeling the endosomal processing in greater details.

Mechanistic difference between LPS and PAM responses

While we argued that NF- κ B pathway induces digital signaling in a series of manuscripts (Tay et al., 2010, Kellogg et al., 2015), the pathway has its analog aspect. For example, cells stimulated by a high dose of TNF α generally exhibit a high peak amplitude (Tay et al., 2010). Similar relation can be observed between LPS dose and the expression levels of downstream genes (Kellogg et al., 2015). We capture this analog aspect in the mathematical model. For example, we simulate the model with various constant levels of activated TRAF6 (TRAF6a) and plot the properties of the first NF-

κ B peak in Figure S2G. The level of TRAF6a characterizes the level of LPS.TLR4 complexes for LPS stimulation and the level of endosomal PAM.TLR2 complexes for PAM stimulation. We find that a high TRAF6a level, induced by a high dose of LPS/PAM, leads to a faster and stronger response. For all levels, the timescale of NF- κ B peaks is 10^1 min.

The time series of NF- κ B activities can be determined by comparing the timescales of TRAF6a accumulation and NF- κ B peaks. For stimulation with a low dose of PAM, cells accumulate TRAF6a in around 200 min (Figure 2A), which is in a slower timescale compared to NF- κ B oscillation. TRAF6a may activate NF- κ B before reaching its maximal level and these peaks are of lower amplitudes than the peak induced by TRAF6 at its maximal level. The miR-146a produced during these peaks is not sufficient to block the pathways (notice the Hill term for miR-146a inhibition). Consequently, we may observe an NF- κ B oscillation of increasing amplitudes. Meanwhile, for stimulation with a high dose of PAM, the timescale of TRAF6a accumulation equals to the timescale of NF- κ B oscillation. The initial peak is triggered when TRAF6a is already around its maximal level and the induced miR-146a rapidly blocks all pathways. Therefore, we observe a single peak response. For LPS stimulation, the initial peak is mediated by MyD88 from the membrane, so there exists no timescale separation and we observe a single peak response.

References

- BRANDT, K. J., FICKENTSCHER, C., KRUITHOF, E. K. O. & DE MOERLOOSE, P. 2013. TLR2 Ligands Induce NF- κ B Activation from Endosomal Compartments of Human Monocytes. *Plos ONE*, 8, e80743.
- GÓMEZ-SJÖBERG, R., LEYRAT, A. A., PIRONE, D. M., CHEN, C. S. & QUAKE, S. R. 2007. Versatile, Fully Automated, Microfluidic Cell Culture System. *Analytical Chemistry*, 79, 8557-8563.
- INVIVOGEN. *Pam3CSK4* [Online]. Available: <http://www.invivogen.com/pam3csk4> [Accessed 06.01 2015].
- KELLOGG, R. A., GÓMEZ-SJÖBERG, R., LEYRAT, A. A. & TAY, S. 2014. High-throughput microfluidic single-cell analysis pipeline for studies of signaling dynamics. *Nature Protocols*, 9, 1713-1726.
- KELLOGG, R. A., TIAN, C., LIPNIACKI, T., QUAKE, S. R. & TAY, S. 2015. Digital signaling decouples activation probability and population heterogeneity. *eLife*, 4, e08931.
- NAHID, M. A., SATOH, M. & CHAN, E. K. L. 2011. MicroRNA in TLR signaling and endotoxin tolerance. *Cellular & Molecular Immunology*, 8, 388-403.
- SIGMA-ALDRICH 2008. *Lipopolysaccharides*, <http://www.sigmaaldrich.com/technical-documents/articles/biology/glycobiology/lipopopolysaccharides.html>.
- TAY, S., HUGHEY, J. J., LEE, T. K., LIPNIACKI, T., QUAKE, S. R. & COVERT, M. W. 2010. Single-cell NF- κ B dynamics reveal digital activation and analogue information processing. *Nature*, 466, 267-271.
- YAO, B., LA, L. B., CHEN, Y.-C., CHANG, L.-J. & CHAN, E. K. L. 2012. Defining a new role of GW182 in maintaining miRNA stability. *EMBO Reports*, 13, 1102-1108.

SUPPLEMENTAL FIGURES

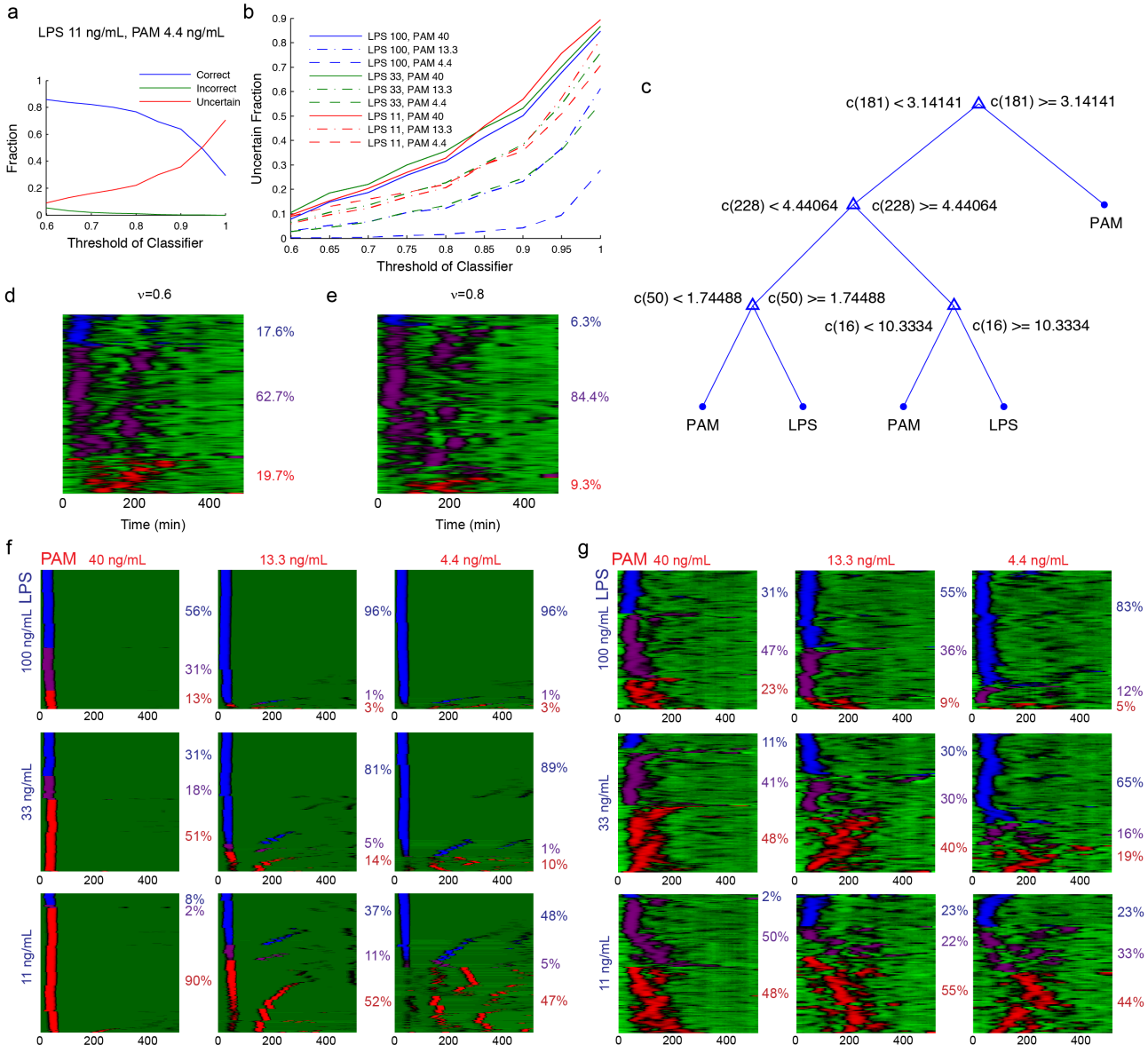


Figure S1. Evaluation of the classifier, related to Figure 1, 3 and 4. (a-b) The effects of the threshold v on the accuracy of bagging classifiers. Each bagging classifier contains 50 decision tree models. (a) For the input condition LPS 11 ng/mL and PAM 4.4 ng/mL, the fractions that the bagging classifiers output correct (blue), incorrect (green) and uncertain (red) labels as a function of threshold v . (b) For all input conditions, the fractions that the bagging classifiers output uncertain labels as a function of threshold v . (c) Example decision tree for LPS 11 ng/mL and PAM 4.4 ng/mL. The symbol $c(t)$ represents the nuclear NF- κ B concentration at t min after stimulation. (d-e) Classification of artificial “mixed” time courses. We restrict to the dose combination of LPS 11 ng/mL and PAM 4.4 ng/mL and create 1000 artificial “mixed” time courses by adding a randomly selected LPS-training trajectory and a randomly selected PAM-training trajectory. Classification of these artificial data is plotted for both (d) $v=0.6$ and (e) $v=0.8$. The percentages represent the fractions of LPS-like (blue), mixed (purple) and PAM-like (red) responses. (f-g) Classification with $N=50$

and $v=0.8$. (f) Classification of model predicted cellular responses under co-stimulation, related to Figure 3D. (g) Classification of experimental cellular responses under co-stimulation, related to Figure 4B.

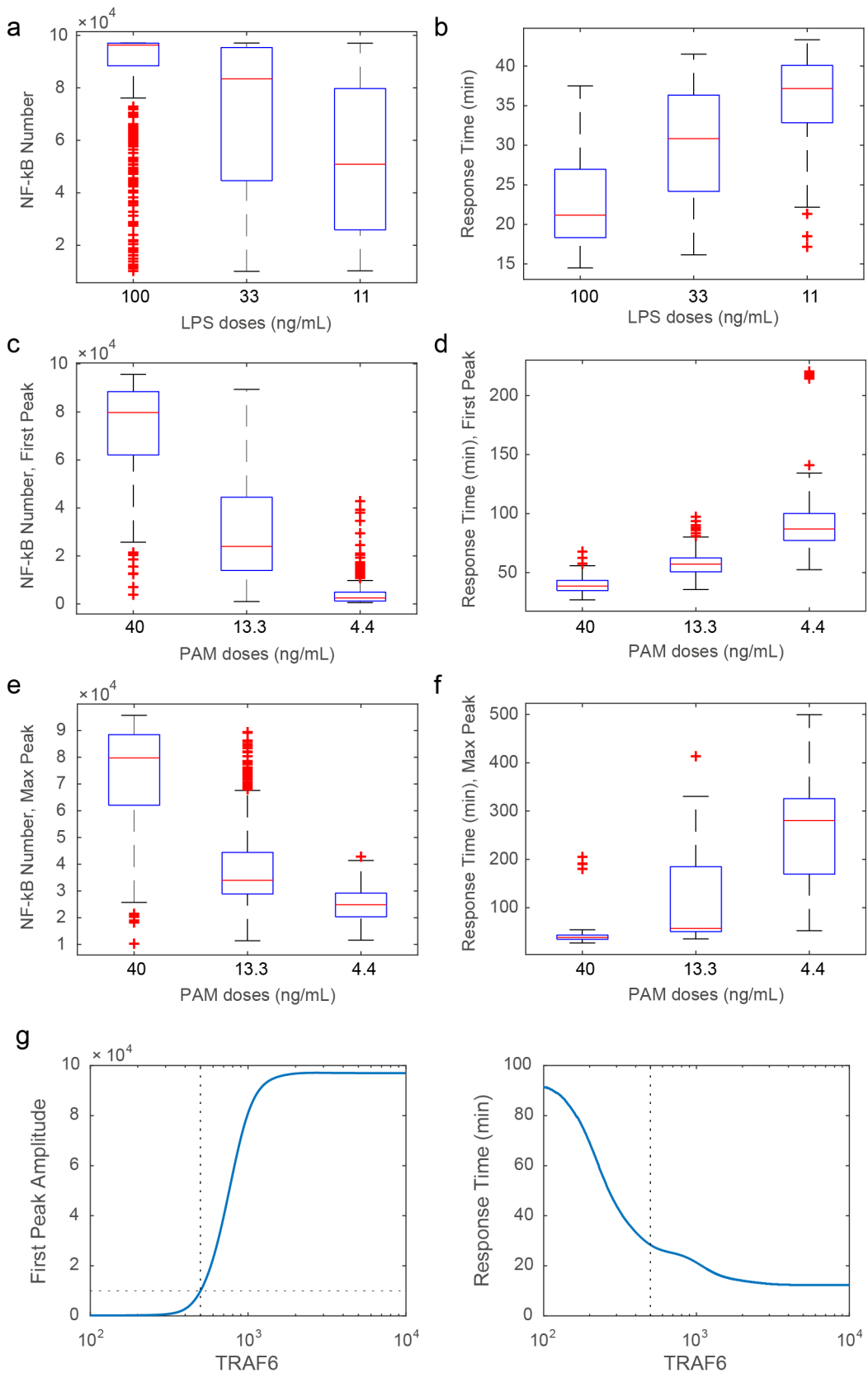


Figure S2. Model evaluation for one ligand, related to Figure 1 and 2. (a-f) Characteristics of simulated cellular responses stimulated by one ligand. (a-b) The characteristics of the first NF-κB peak under LPS stimulus; (c-d) The

characteristics of the first NF- κ B peak under PAM stimulus; (e-f) The characteristics of the maximal NF- κ B peak under PAM stimulus. (a,c,e) The distribution of the amplitudes of the NF- κ B peaks. The total number of NF- κ B in the cells is 10^5 . (b,d,f) The distribution of the response times of the NF- κ B peaks. 500 independent simulations are used to compute the distributions. Only active trajectories (more than 10% of NF- κ B enters the cells) are considered. The model-predicted response times show good consistency with the experimental data, while the model produces a strong dependency between peak amplitudes and doses which is less strong in the experiments. (g) Relationship between a constant TRAF6a level and the properties of the first NF- κ B peak. The dash line represents the threshold for activation.

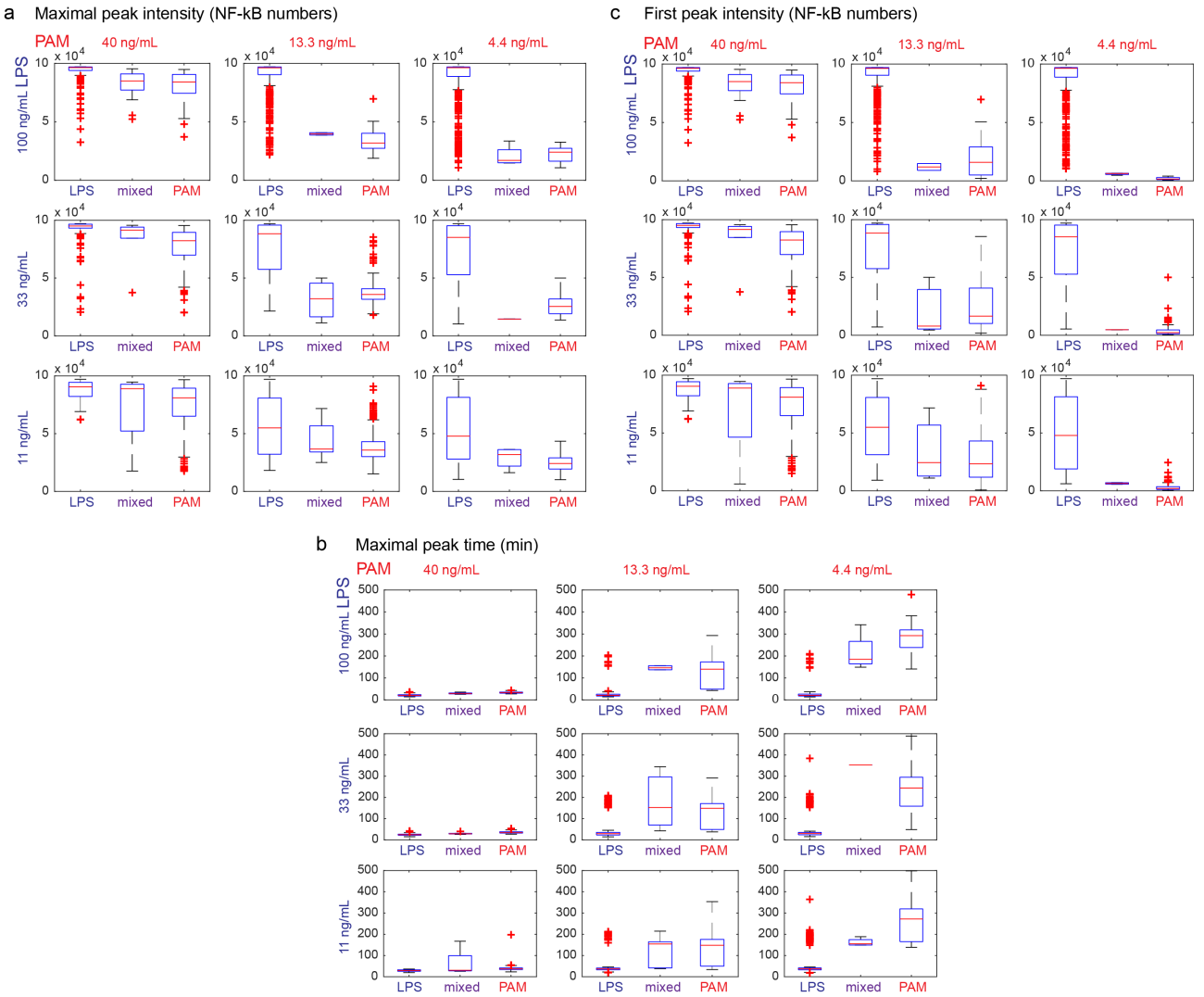


Figure S3. Model evaluation for co-stimulation, related to Figure 3. (a) Distribution of maximal NF- κ B peak amplitudes. For each input condition, we simulate 500 trajectories and use classifier to classify all trajectories into LPS-like, PAM-like and mixed type. We then plot the distribution of the maximal peak amplitude for each category in the form of box plots. Only active trajectories are considered. Vertical axis represents the amplitude of the maximal peak in NF- κ B numbers. The total number of NF- κ B in the cells is 10^5 . (b) Distribution of the maximal NF- κ B peak response times. Vertical axis represents the response time of the maximal peak in minutes. (c) Distribution of the first NF- κ B peak amplitudes. The characteristics for LPS-like and PAM-like trajectories generally show good agreement with cellular responses under single stimulation (Figure S2).

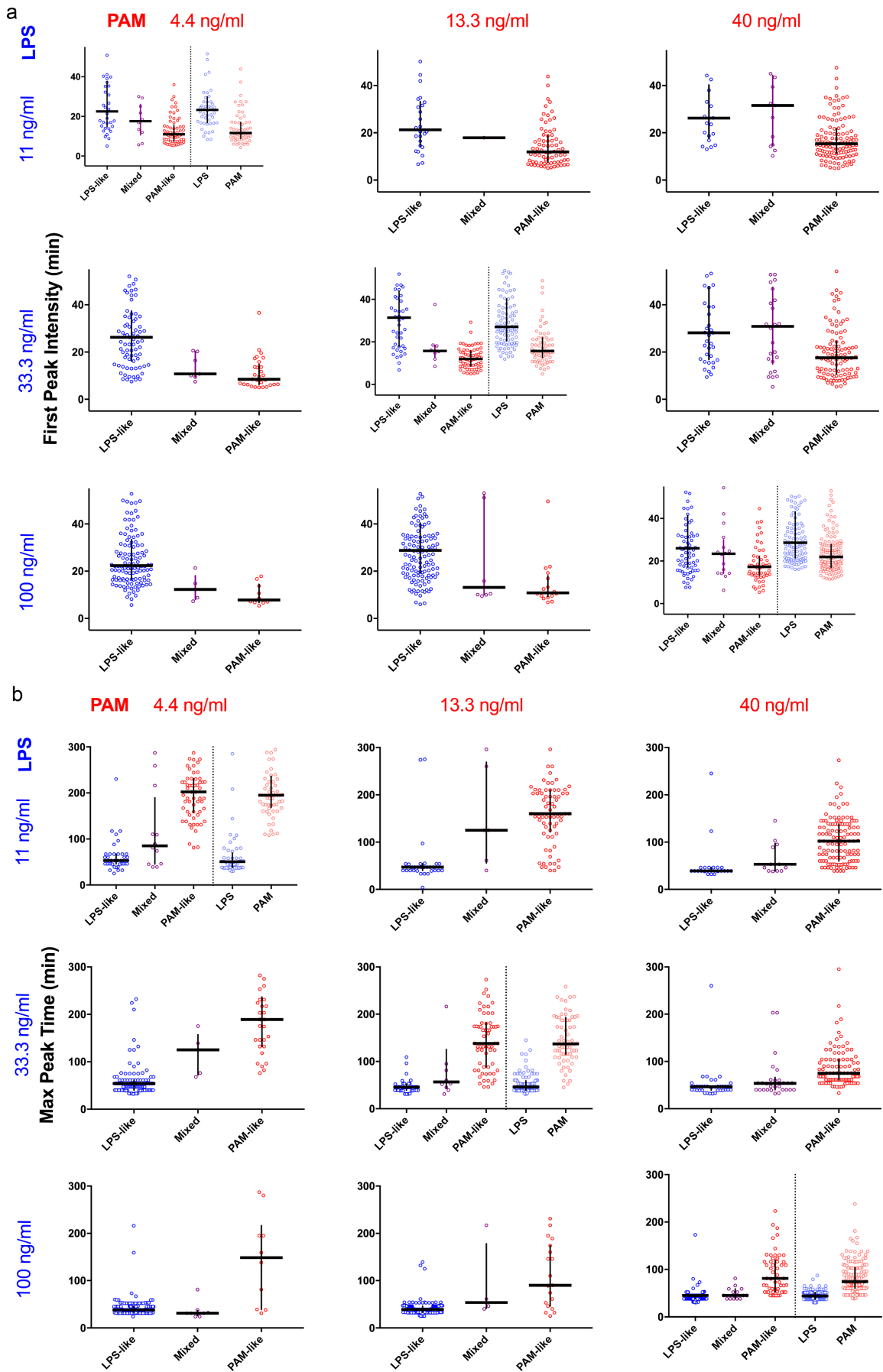


Figure S4. Evaluation of experimental cellular responses under co-stimulation, related to Figure 4. Experimental data are classified into “LPS-like”, “PAM-like” and “mixed” and plotted in the style of Figure 1C-D. We reproduce the data points in Figure 1C-D in “LPS” and “PAM” columns for comparison. (a) Distribution of first NF- κ B peak amplitudes. Vertical axis represents the amplitude of the first peak in arbitrary units. The panel for LPS 11 ng/mL and PAM 4.4 ng/mL is reproduced from Figure 4D. (b) Distribution of maximal NF- κ B peak response times. Vertical axis represents the response time of the maximal peak in minutes. The panel for LPS 11 ng/mL and PAM 4.4 ng/mL is reproduced from Figure 4E.

SUPPLEMENTAL TABLES

Table S1. The accuracy of the bagging classifiers, related to Figure 1.

	$N=10$	$N=15$	$N=20$	$N=30$	$N=40$	$N=50$
$v=0.60$	0.90	0.89	0.89	0.89	0.89	0.89
$v=0.65$	0.85	0.86	0.87	0.86	0.87	0.86
$v=0.70$	0.85	0.83	0.85	0.84	0.84	0.84
$v=0.75$	0.79	0.78	0.82	0.80	0.81	0.80
$v=0.80$	0.79	0.78	0.77	0.77	0.77	0.77
$v=0.85$	0.70	0.71	0.73	0.70	0.71	0.70
$v=0.90$	0.70	0.62	0.66	0.64	0.64	0.63
$v=0.95$	0.52	0.46	0.56	0.49	0.53	0.49
$v=1.00$	0.52	0.46	0.41	0.36	0.32	0.30

Table S2. Quality assessment of the classifier for classifying single-stimulus time courses, related to Figure 1. $N=50$, $\nu=0.6$. The quantities are evaluated by 10-fold CV. AUROC and AUPR are computed without the assignment of the uncertain label. The AUPR value is for reference only as the composition of the test data may vary in different CV runs. C, I and U stand for Correct, Incorrect and Uncertain labels.

Dose (LPS-PAM, ng/mL)	LPS responses			PAM responses			AUROC	AUPR
	C	I	U	C	I	U		
100-40	0.84	0.07	0.09	0.87	0.05	0.08	0.96	0.78
100-13.3	0.97	0.02	0.02	0.88	0.07	0.05	0.99	0.54
100-4.4	1.00	0.00	0.00	1.00	0.00	0.00	1.00	0.21
33-40	0.75	0.12	0.13	0.87	0.04	0.09	0.95	0.75
33-13.3	0.90	0.05	0.05	0.83	0.09	0.08	0.97	0.66
33-4.4	0.95	0.04	0.01	0.95	0.01	0.03	0.99	0.37
11-40	0.59	0.20	0.21	0.94	0.01	0.06	0.93	0.63
11-13.3	0.84	0.10	0.06	0.89	0.06	0.05	0.97	0.64
11-4.4	0.83	0.08	0.09	0.89	0.02	0.09	0.98	0.57

Table S3. Statistics of the example decision tree, related to Figures 1 and S1.

Split	Importance	LPS labels to classify	PAM labels to classify
c(181)	0.0851	48	60
c(228)	0.0220	48	10
c(50)	0.0058	46	2
c(16)	0.0074	2	8

Table S4. Mathematical model, related to Figure 2.

TLR4-mediated signaling		TLR2-mediated signaling	
$LPS \rightarrow \emptyset$	Degradation of LPS	$PAM \rightarrow \emptyset$	Degradation of PAM
$l_a[LPS]$		$p_a[PAM]$	
$LPS + TLR4 \rightarrow LPS.TLR4$	Binding of LPS and TLR4	$PAM + TLR2 \rightarrow PAM.TLR2$	Binding of PAM and TLR2
$l_b[LPS][TLR4]$		$p_b[PAM][TLR2]$	
$LPS.TLR4 \rightarrow LPS + TLR4$	Unbinding of LPS and TLR4	$PAM.TLR2 \rightarrow PAM + TLR2$	Unbinding of PAM and TLR2
$l_f[LPS.TLR4]$		$p_f[PAM.TLR2]$	
$TRAFF6 \rightarrow TRAF6a(LPS)$	Activation of TRAF6a by LPS.TLR4	$TRAFF6 \rightarrow TRAF6a(PAM)$	Activation of TRAF6a by PAM.TLR2
$l_a[LPS.TLR4][TRAFF6] * \frac{k_{M,A20(LPS)}^4}{k_{M,A20(LPS)} + [A20] [miR146a]^4 + k_{M,miR146a(LPS)}^4}$		$p_a[PAM.TLR2][TRAFF6] * \frac{k_{M,A20(PAM)}^4}{k_{M,A20(PAM)} + [A20] [miR146a]^4 + k_{M,miR146a(PAM)}^4}$	
$TRAFF6a(LPS) \rightarrow TRAF6$	Inactivation of TRAF6a	$TRAFF6a(PAM) \rightarrow TRAF6$	Inactivation of TRAF6a
$l_i[TRAFF6a(LPS)]$		$p_i[TRAFF6a(PAM)]$	
miR-146a related signaling			
$MIR146A \text{ gene off} \rightarrow \text{on}$		Activation of the MIR146a gene	
$g_{1,miR146a}[NF\kappa B.\text{nuc}][miR146a \text{ gene off}]$			
$MIR146A \text{ gene on} \rightarrow \text{off}$		Inactivation of the MIR146a gene	
$g_{2,miR146a}[I\kappa B\alpha.\text{nuc}][miR146a \text{ gene on}]$			
$\emptyset \rightarrow miR - 146a$		Synthesis of miR-146a	
$g_{tsc,miR146a}[miR146a \text{ gene on}]$			
$miR - 146a \rightarrow \emptyset$		Degradation of miR-146a	
$d_{,miR146a}[miR146a]$			

Table S5. Parameter values, related to Figure 2.

TLR4-mediated signaling		TLR2-mediated signaling	
μ_l	Mean parameter of TLR4 distribution	μ_p	Mean parameter of TLR2 distribution
8.0	(Kellogg et al., 2015)	8.0	Assume same as LPS pathway
σ_l	Standard deviation parameter of TLR4 distribution	σ_p	Standard deviation parameter of TLR2 distribution
0.8	(Kellogg et al., 2015)	0.4	Fitted
l_d	Degradation rate of LPS	p_d	Degradation rate of PAM
5×10^{-4}	(Kellogg et al., 2015)	1×10^{-5}	Fitted
l_b	Binding rate between LPS and TLR4	p_b	Binding rate between PAM and TLR2
1×10^{-9}	Fitted	5×10^{-11}	Fitted
l_f	Unbinding rate between LPS and TLR4	p_f	Unbinding rate between PAM and TLR2
5×10^{-4}	Rounded from (Kellogg et al., 2015)	1×10^{-6}	Fitted
l_a	Activation rate of TRAF6 by LPS.TLR4	p_a	Activation rate of TRAF6 by PAM.TLR2
1×10^{-7}	(Kellogg et al., 2015)	1×10^{-7}	Assume same as LPS pathway
$k_{M,A20(LPS)}$	Michaelis-Menten constant for the inhibitory effect of A20	$k_{M,A20(PAM)}$	Michaelis-Menten constant for the inhibitory effect of A20
10^5	(Kellogg et al., 2015)	10^5	Assume same as LPS pathway
$k_{M,miR146a(LPS)}$	Hill constant for the inhibitory effect of miR-146a	$k_{M,miR146a(PAM)}$	Hill constant for the inhibitory effect of miR-146a
6×10^2	Fitted	6×10^2	Assume same as LPS pathway
l_i	Inhibition rate of TRAF6a(LPS)	p_i	Inhibition rate of TRAF6a(PAM)
1×10^{-2}	(Kellogg et al., 2015)	1×10^{-2}	Assume same as LPS pathway
$c_{1(LPS)}$	Activation rate of IKK by TRAF6a(LPS)	$c_{1(PAM)}$	Activation rate of IKK by TRAF6a(PAM)
2×10^{-2}	(Kellogg et al., 2015)	2×10^{-2}	Assume same as LPS pathway
$K_{TRAF6a(LPS)}$	Hill constant for the activation of IKK by TRAF6a(LPS)	$K_{TRAF6a(PAM)}$	Hill constant for the activation of IKK by TRAF6a(PAM)
3.5×10^3	(Kellogg et al., 2015)	3.5×10^3	Assume same as LPS pathway
miR-146a related signaling			
$g_{1,miR146a}$	Activation rate of MIR146A genes	1×10^{-7}	Fitted
$g_{2,miR146a}$	Inactivation rate of MIR146A genes	2×10^{-6}	Fitted
$g_{tsc,miR146a}$	Synthesis rate of miR-146a	0.5	Fitted
$d_{miR146a}$	Degradation rate of miR-146a	2×10^{-5}	Assume 5 h half-life, support from (Yao et al., 2012)

Table S6. Fraction of active cells of the simulated and experimentally measured cellular responses, related to Figure 1-4.

Input Condition	Experimental Trajectories	Simulated Trajectories
LPS 100 ng/mL	0.95	0.974
LPS 33 ng/mL	0.73	0.852
LPS 11 ng/mL	0.47	0.472
PAM 40 ng/mL	1.00	1.000
PAM 13.3 ng/mL	1.00	1.000
PAM 4.4 ng/mL	1.00	0.950
LPS 100 ng/mL, PAM 40 ng/mL	1.00	1.000
LPS 100 ng/mL, PAM 13.3 ng/mL	1.00	1.000
LPS 100 ng/mL, PAM 4.4 ng/mL	1.00	0.998
LPS 33 ng/mL, PAM 40 ng/mL	1.00	1.000
LPS 33 ng/mL, PAM 13.3 ng/mL	1.00	1.000
LPS 33 ng/mL, PAM 4.4 ng/mL	1.00	0.996
LPS 11 ng/mL, PAM 40 ng/mL	1.00	1.000
LPS 11 ng/mL, PAM 13.3 ng/mL	1.00	1.000
LPS 11 ng/mL, PAM 4.4 ng/mL	1.00	0.982

Table S7. The fraction of LPS-, PAM- and mixed-type responses, related to Figure 3D.

Input Condition	LPS	PAM	Uncertain
LPS 100 ng/mL, PAM 40 ng/mL	83%	14%	4%
LPS 100 ng/mL, PAM 13.3 ng/mL	96%	4%	0%
LPS 100 ng/mL, PAM 4.4 ng/mL	96%	3%	0%
LPS 33 ng/mL, PAM 40 ng/mL	34%	53%	14%
LPS 33 ng/mL, PAM 13.3 ng/mL	83%	15%	1%
LPS 33 ng/mL, PAM 4.4 ng/mL	89%	10%	0%
LPS 11 ng/mL, PAM 40 ng/mL	8%	91%	1%
LPS 11 ng/mL, PAM 13.3 ng/mL	42%	56%	2%
LPS 11 ng/mL, PAM 4.4 ng/mL	51%	48%	1%

Table S8. Statistical analysis comparing NF-κB peak characteristics under co-stimulation, related to Figure 4. For all dose combinations, first peak intensity and maximum peak time are statistically different between “LPS-like” and “PAM-like” classes by Mann-Whitney test.

Input Condition	First Peak Intensity	Max Peak Time
	<i>LPS-like vs. PAM-like (p value)</i>	<i>LPS-like vs. PAM-like (p value)</i>
LPS 100 ng/mL + PAM 40 ng/mL	<0.0001	<0.0001
LPS 100 ng/mL + PAM 13.3 ng/mL	<0.0001	<0.0001
LPS 100 ng/mL + PAM 4.4 ng/mL	<0.0001	0.011
LPS 33 ng/mL + PAM 40 ng/mL	<0.0001	<0.0001
LPS 33 ng/mL + PAM 13.3 ng/mL	<0.0001	<0.0001
LPS 33 ng/mL + PAM 4.4 ng/mL	<0.0001	<0.0001
LPS 11 ng/mL + PAM 40 ng/mL	<0.0001	<0.0001
LPS 11 ng/mL + PAM 13.3 ng/mL	<0.0001	<0.0001
LPS 11 ng/mL + PAM 4.4 ng/mL	<0.0001	<0.0001

Table S9. Statistical analysis of comparing NF-κB peak characteristics of classified as LPS-like (PAM-like) under co-stimulation to LPS (PAM) alone, related to Figure 4. In all cases there is *not* a significant difference in first peak intensity and maximum peak time in cells classified as LPS-like (PAM-like) under co-stimulation compared to LPS (PAM) stimulation alone.

Input Condition	First Peak Intensity (p value)	Max Peak Time (p value)
	<i>LPS-like vs. LPS</i>	<i>PAM-like vs. PAM</i>
LPS 100 ng/mL + PAM 40 ng/mL	0.4543	0.8295
LPS 33 ng/mL + PAM 13.3 ng/mL	0.2064	0.9593
LPS 11 ng/mL + PAM 4.4 ng/mL	0.1545	0.8273